

UNIVERSITY OF GRONINGEN

KAPTEYN ASTRONOMICAL INSTITUTE  
&  
KVI ATOMIC AND MOLECULAR PHYSICS

MSc PROJECT

---

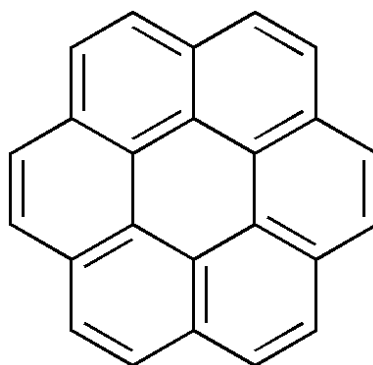
Hydrogen Addition to Polycyclic Aromatic  
Hydrocarbons

---

The First Step to the Formation of H<sub>2</sub> in Space

*by*

L.M.P.V. BOSCHMAN



*Supervisors*

KAPTEYN  
Dr. Stéphanie CAZAUX  
Prof. Dr. Marco SPAANS

KVI  
Drs. Geert REITSMA  
Dr. Thomas SCHLATHÖLTER  
Prof. Dr. Ir. Ronnie HOEKSTRA

## Abstract

Molecular hydrogen is the most abundant molecule in the Universe and a large portion of it is formed by hydrogen atoms that are adsorbed on polycyclic aromatic hydrocarbons (PAHs). The rate of this formation route depends strongly on the H sticking probability. In this study we irradiate coronene cations with hydrogen atoms to study the catalysis of H<sub>2</sub>-formation by PAHs. We observe a systematic increase with irradiation time of the number of hydrogen atoms attached to the coronene cation. We also find that the states with an odd number of hydrogen atoms dominate the mass spectrum up to 11 H atoms. This indicates the presence of a barrier at every second hydrogenation of the coronene cation. We estimate the barrier of the second hydrogenation to be  $72 \pm 6$  meV and the one for the fourth hydrogenation is determined at  $40 \pm 10$  meV. These results are in good agreement with theoretical predictions for the hydrogenation of neutral PAHs. The alternating behaviour for the barrier continues to exist for the higher hydrogenation states, implying that the barrier does not vanish for higher hydrogenation states. These results indicate that PAH cations, like their neutral counterparts, exist in highly hydrogenated forms in the ISM. Due to their catalytic activity, PAH cations and neutrals seem to contribute similarly to the formation of H<sub>2</sub>.

<b>1</b>	<b>Introduction</b>	<b>4</b>
1.1	Star formation . . . . .	4
1.2	The H <sub>2</sub> problem . . . . .	5
1.3	Polycyclic aromatic hydrocarbons . . . . .	6
1.4	Previous work . . . . .	8
1.5	This project . . . . .	9
<b>2</b>	<b>Theory</b>	<b>10</b>
2.1	Hydrogen addition to coronene . . . . .	10
2.2	Kinetics of hydrogen addition . . . . .	11
<b>3</b>	<b>Experimental setup</b>	<b>15</b>
3.1	Electrospray ionisation . . . . .	15
3.2	Ion funnel . . . . .	16
3.3	Ion mass filter . . . . .	18
3.4	Paul ion trap . . . . .	21
3.5	Mass spectrometry . . . . .	21
3.6	Atomic hydrogen source . . . . .	22
<b>4</b>	<b>Experimental procedure</b>	<b>24</b>
4.1	Sample preparation . . . . .	24
4.2	Operational procedure . . . . .	25
<b>5</b>	<b>Results</b>	<b>27</b>
5.1	Raw data . . . . .	27
5.2	Observed trends . . . . .	29
<b>6</b>	<b>Data analysis</b>	<b>30</b>
6.1	Line evolution . . . . .	30

6.2	Deriving energy barriers . . . . .	34
<b>7</b>	<b>Discussion</b>	<b>37</b>
7.1	Summary . . . . .	37
7.2	Comparison with previous work . . . . .	37
7.3	Consequences for H <sub>2</sub> formation . . . . .	39
7.4	Outlook . . . . .	39
<b>8</b>	<b>Conclusion</b>	<b>41</b>
<b>9</b>	<b>Acknowledgements</b>	<b>42</b>
<b>A</b>	<b>Mass spectra</b>	<b>47</b>
<b>B</b>	<b>Paper</b>	<b>71</b>

# CHAPTER 1

## Introduction

Until very recently, stars were thought to be eternal, unchanging sources of light. People considered stars to be deities or, like the Romans, thought that they were pinholes in the veil that shielded us from the heaven where the gods lived. As human knowledge progressed, stars have been demoted from their divine status to that of giant balls of glowing gas. Initially people still thought that stars had existed as long as time itself, but soon it became clear that stars are born, change and die just like mortals.

Ever since mankind discovered the true nature of stars, these processes have been subject of vigorous research and investigation, leading to many a theory about the birth, life and death of stars. To encompass all these stages is beyond the scope of this project, so we will now focus on the phase relevant for this thesis, the formation of stars.

### 1.1 Star formation

For a star to be born, a lot of gas has to be accumulated into a relatively small volume. This is possible when a gas cloud collapses after it has crossed the Jeans stability limit, i.e. it is heavier than the Jeans mass corresponding to its temperature and density. As soon as that limit is reached, the cloud is no longer able to support its own weight with its internal pressure, and the cloud collapses under its own weight. Before this collapse can happen, a molecular cloud has to form dense cores who can then turn into stars. For this process to happen, efficient cooling of the molecular cloud is necessary. The cooling agent present defines the efficiency of this cooling and thus of the star formation, as well as the characteristics of the stars formed (mass and binarity).

Star formation happens primarily in molecular clouds, which are cold regions of the interstellar medium (ISM) with a temperature of  $T \approx 20$  K

(Wolfire et al. 2003; Norman and Spaans 1997). With gas number densities of  $n \approx 10^4 - 10^5 \text{ cm}^{-3}$ , these clouds are gravitationally bound and they possess dense cores ( $10^6 \text{ cm}^{-3}$ ) that lead to star formation.

The most dominant molecule in these molecular clouds is the hydrogen molecule  $\text{H}_2$ . Via several heating and cooling pathways this molecule has a large influence on the thermal energy budget of the gas cloud, and therefore on the process of star formation.

$\text{H}_2$  can heat the gas through photodissociation by UV irradiation. Another heating method is collisional de-excitation of an  $\text{H}_2$ -molecule that is vibrationally excited upon formation or after radiative excitation (Tielens 2005).

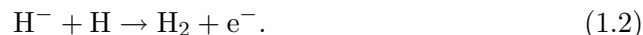
$\text{H}_2$  has cooling properties as well, via collisional vibrational excitation and subsequent radiative de-excitation. The formation of the first stars was probably possible due to cooling by molecular hydrogen (Norman and Spaans 1997).

Furthermore, molecular hydrogen is important as cooling agent in shocks, low metallicity galaxies and other warm gas regions where other cooling agents are of little importance (Cazaux 2004).

Because of its abundance, it is also involved in a plethora of chemical pathways, enhancing the complexity of the ISM chemistry. Reactions of  $\text{H}_2$  with other species, both neutral and ionized, can lead to the formation of cooling agents, such as CO, OH and  $\text{H}_2\text{O}$  (Meijerink and Spaans 2005).

## 1.2 The $\text{H}_2$ problem

The most abundant molecule in molecular clouds is the hydrogen molecule,  $\text{H}_2$ . The gas phase route to the formation of this molecule is an indirect one, because the direct formation out of two single hydrogen atoms is impossible due to conservation of energy. One needs either a three-body collision or another process to dissipate the excess energy. The most common process uses a surplus electron to get rid of the momentum. The dominant gas phase  $\text{H}_2$ -formation process is then summarized in equations (1.1) and (1.2).



This formation route has a reaction rate that depends on the ionization of the ISM (Tielens 2005) which is given by

$$R(\text{H}_2) = 1.3 \times 10^{-9} n(\text{H}^-) n(\text{H}) \text{ cm}^{-3} \text{ s}^{-1}. \quad (1.3)$$

Observations of molecular clouds have revealed that there is much more  $\text{H}_2$  present than can be accounted for by gas-phase chemistry alone. Based

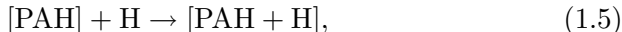
on these observations, an actual H<sub>2</sub>-formation rate has been found that is several orders of magnitude larger than the gas-phase chemistry predictions (Tielens 2005). This H<sub>2</sub> excess can be explained by a formation route where interstellar dust surfaces catalyze the necessary chemical reactions (Oort and van de Hulst 1946; Gould and Salpeter 1963).

Observations of diffuse clouds allowed to derive direct H<sub>2</sub>-formation rates on dust grains, which have become the canonical value used in astrophysical models. This rate has a typical value of  $1 - 3 \times 10^{-17} \text{cm}^3 \text{s}^{-1}$  and can be written as

$$R_d(H_2) = \frac{1}{2}n(\text{H})v_{\text{H}}n_{\text{grain}}\sigma\epsilon_{\text{H}_2}S(T), \quad (1.4)$$

where  $n(\text{H})$ , is the number densities of H atoms in the gas phase,  $v_{\text{H}}$  is the thermal velocities of H atoms calculated as  $\sqrt{\frac{8\pi kT}{m_{\text{H}}}}$ ,  $\epsilon_{\text{H}_2}$ , is the formation efficiency of H<sub>2</sub>.  $S(T)$  is the sticking coefficient. The mean cross section for collisions between grains and atoms,  $n_{\text{grain}}\sigma$ , is determined as  $\langle \frac{n_{\text{grain}}(a)}{n_{\text{H}}}\pi a^2 \rangle$  with  $n_{\text{grain}}(a)$  the grain density with radius between  $a$  and  $a+\Delta a$ .

The surface area available for chemistry ( $n_{\text{grain}}\sigma$ ) is provided by dust and polycyclic aromatic hydrocarbons (PAHs). These PAHs are large, graphitic carbon molecules and make up 50 % of the available surface area (Weingartner and Draine 2001). The catalysis of H<sub>2</sub>-formation by PAHs is described in equations (1.5) and (1.6).



### 1.3 Polycyclic aromatic hydrocarbons

For this project we study polycyclic aromatic hydrocarbons, which are large graphite-like molecules of carbon atoms arranged in a hexagonal pattern. This gives the molecule a planar, honeycomb structure and due to the aromatic carbon bonds, they are very stable molecules. These PAHs come in various sizes, where the smallest is the two-ring system naphthalene. Larger PAHs also exhibit a certain irregularity in their overall shape, while they still maintain their almost lattice-like atom configuration as shown in figure 1.1. In this study we focus our attention to one particular PAH, coronene, since this molecule is widely commercially available.

Consisting of 24 carbon atoms, coronene is an intermediate between the two extreme sizes of PAHs. It is named after its crown-like structure of six benzene rings surrounding a seventh one and has a large degree of symmetry, as shown in figure 1.2.

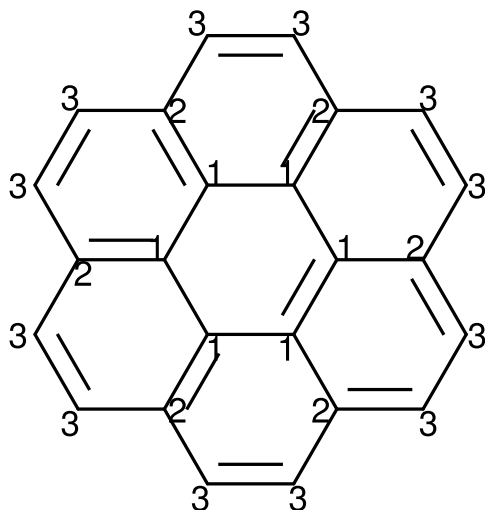


Figure 1.2: The coronene molecule ( $C_{24}H_{12}$ ). Labels have been added to all central (1), edge (2) and outer edge (3) carbon atoms.

Although it is a relatively small PAH, it is large enough to exhibit some of the chemical and physical features observed in the larger PAHs. One of these features is the presence of three chemically different carbon atoms as shown in figure 1.2: the central (1), edge (2) and outer edge (3) carbon atoms. The outer edge atoms are those that have formed a bond with a hydrogen atom and they are usually found at the perimeter of a PAH molecule. Edge carbon atoms are to be found on the perimeter as well, but they do not have a bond with a hydrogen atom. Instead, they are neighbouring the outer edge carbon atoms. The central carbon atoms are found in the central regions and only possess bonds with other central or edge carbon atoms. These three categories of carbon atoms differ significantly in their chemical properties, such as the activation energy for hydrogen addition.

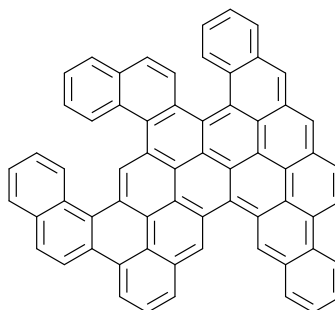


Figure 1.1: A large, irregular PAH.

### Coronene and $H_2$ formation

For this project we study the role of coronene in the catalysis of  $H_2$  formation. The most important mechanism for the catalyzed formation of  $H_2$  happens in two steps via the so-called Eley-Rideal mechanism. First, a hydrogen atom from the gas phase bonds with a PAH molecule to form a hydrogenated PAH. A second hydrogen atom can then abstract this H atom

from the PAH and form a hydrogen molecule.

The rate limiting step in this process is the first one, because it is the most difficult one. The barrier that the incoming hydrogen atom must overcome is much higher than for the second step (Rauls and Hornekær 2008). In this study we explore the first step of the catalysis experimentally by studying the hydrogenation of coronene cations after irradiation with hydrogen atoms. We use coronene as a probe molecule for PAHs, because it is large enough to exhibit the dynamics that govern the behaviour of large PAHs, but it is still small enough to be easily handled.

## 1.4 Previous work

The interstellar relevance of PAHs is a field where theory and experiment go hand in hand. Most of the studies performed focus on coronene for the same reasons as stated above. For example, Rauls and Hornekær (2008) derive barriers for the addition of H atoms to neutral coronene using density functional theory calculations. They find that the barrier depends strongly on the location of the addition. Hydrogen addition to the outer edge carbon atoms has an energy barrier of 60 meV compared to approximately 200 meV for addition to the other carbon atoms. Rauls and Hornekær (2008) also find that hydrogen addition to an outer edge carbon atom next to an already hydrogenated outer edge carbon atom is barrierless. This is in accordance with calculations done by Bauschlicher (1998), who found that for smaller PAHs hydrogenation takes place preferentially next to already hydrogenated carbon atoms.

Mennella et al. (2012) irradiate coronene films with D atoms and find proof for both addition and abstraction. They do this by measuring the intensity of the aromatic C-H band and the aliphatic C-H band after different doses of D irradiation. Thrower et al. (2012) thermally desorb a coronene film after exposure to a dose of D atoms. This evaporated film is analyzed with a quadrupole mass spectrometer to measure the number of D atoms attached to each coronene molecule. With this method they find super-hydrogenated coronene molecules where even the central carbon atoms are hydrogenated, although this has a much larger energy barrier (Rauls and Hornekær 2008).

Experiments with gas-phase PAHs (Snow et al. 1998; Betts et al. 2006) are predominantly performed with PAH cations. Snow et al. (1998) find that small PAH cations react very efficiently with atomic hydrogen, oxygen and nitrogen. They conclude that cationic PAHs are therefore unlikely to be observed in the ISM, but that one should look for protonated PAHs instead. Betts et al. (2006) perform similar measurements and include the coronene cation as well. Both studies are able to determine rate constants for the first hydrogenation.

## 1.5 This project

For this study we perform experiments at the Zernike-LEIF facility at the KVI Atomic and Molecular Physics group. We use the Paultje setup to bring coronene cations in the gas phase and trap them in a Paul ion trap. The ions are then irradiated with a room temperature beam of atomic hydrogen. Subsequently performing mass spectrometry of the trap contents allows us to study the addition of hydrogen atoms to the coronene cations.

We present the detection of multiply hydrogenated coronene cations after irradiation with room temperature H atoms. We find that every second hydrogenation of the coronene cation has an associated barrier and that this holds up to high hydrogenation states. Finally, we are able to determine the height of these barriers at the second and the fourth hydrogenation and measure them to be  $72 \pm 6$  meV and  $40 \pm 10$  meV, respectively.

From the existence of these barriers we infer that the reaction rates for PAH-catalyzed H<sub>2</sub> formation have a strong temperature dependence in the astrophysically relevant temperature regime.

There is a lot of theory behind the experiments in this project. For example, there are the chemical reactions taking place and the mechanisms that drive them. These mechanisms come with certain kinetics that govern the rate at which they are happening. There is also the theory behind the components of the experimental setup, which is described in chapter 3. This chapter tries to provide a theoretical background to the chemical reactions between hydrogen and coronene.

## 2.1 Hydrogen addition to coronene

When it comes to hydrogen addition to coronene, one can distinguish three different locations for the hydrogen atom to stick, the central carbon atoms, edge carbon atoms and outer edge carbon atoms (Rauls and Hornekær 2008). They differ from each other in their respective reaction energies and barriers.

The addition of hydrogen to a central carbon atom is a reaction that has an energy barrier. This energy barrier is due to the so-called puckering of the carbon atom the hydrogen attaches to as it changes its electronic hybridization from  $sp^2$  to  $sp^3$ . This change of hybridization is necessary, because the three  $sp^2$  orbitals of the C atom are already involved in chemical bonds and an H atom cannot form a bond through overlap with the remaining p-orbital. As the hybridization changes, so does the spatial conformation of the covalent bonds formed by the changing C atom. An  $sp^2$  hybridized C atom has its  $sp^2$  orbitals lying in one plane with the remaining p-orbital perpendicular to that plane, whereas an  $sp^3$  C atom has its four  $sp^3$  orbitals in a tetrahedral orientation. If the C atom is already covalently bonded to three other C atoms in the coronene molecule, the change of hybridization causes the C atom to move out of the molecular plane. Because of this movement, the orbital overlap between this C atom and its direct

neighbours decreases. This so-called conformational stress gives rise to an energy barrier of 200 meV (Rauls and Hornekær 2008) that has to be overcome before the addition reaction can take place and therefore reduces the rate at which the reaction is occurring.

The edge and central carbon atoms are all surrounded by three other C atoms. In the case of the central atoms, the C atoms that surround them are in turn surrounded by three other C atoms, leading to even less conformational freedom than in the case of the edge C atoms.

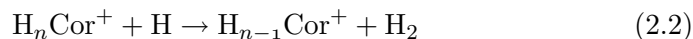
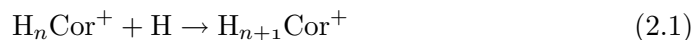
The outer edge carbon atoms are only bound to two other C atoms and the remaining hydrogen atom can move freely during the hybridization transformation from  $sp^2$  to  $sp^3$ . This reduces the conformational stress significantly, making the outer edge carbon atoms the preferred hydrogenation site.

Rauls and Hornekær (2008) calculate the height of the barriers associated to hydrogenation of neutral coronene molecules and confirm that the first hydrogenation experiences the lowest barrier at an outer edge carbon atom. They also find that hydrogen addition to the outer edge carbon atom immediately next to the first hydrogenation site does not have a barrier. Calculations by others support this preference for outer edge hydrogenation next to hydrogenated outer edge carbon atoms (Bauschlicher 1998). It is therefore expected that every second outer edge hydrogenation of a neutral coronene molecule is barrierless.

For practical reasons we are using radical cations instead of neutral molecules, so these calculations are not entirely valid anymore. However, the second hydrogenation of the cation is electronically equivalent to the first hydrogenation of the neutral molecule. We therefore expect that every second hydrogenation of the cation has a barrier, while the odd-numbered hydrogenations can happen unobstructed, as depicted in figure 2.1. This implies that the cations remain longer in odd hydrogenation states, since it is more difficult to hydrogenate further from one of those states.

## 2.2 Kinetics of hydrogen addition

To interpret our experimental results better, we use a kinetic chemical model. In this model we incorporate both hydrogen addition and hydrogen abstraction reactions, which can be described as



We start the model with the coronene cation as the only present molecule, which is then hydrogenated via a barrierless reaction with rate constant  $k_1 = A_1$ . Then we treat the site that is initially hydrogenated as chemically

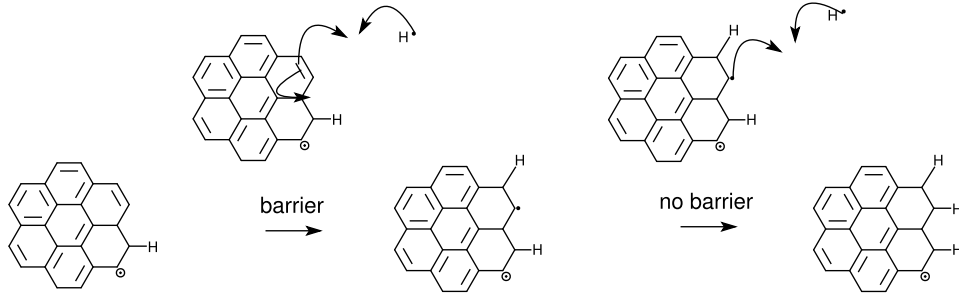


Figure 2.1: A schematic drawing of the second and third hydrogenation steps. The molecule on the left is the coronene cation with one hydrogen atom already attached. The first incoming H atom experiences a barrier to hydrogenate this molecule, while the second H atom can hydrogenate without a barrier.

inactive. The next hydrogenation takes place preferably at one of the outer edge sites adjacent to the already hydrogenated outer edge site.

This leaves four outer edge carbon atoms where the first step of further hydrogenation can take place with a rate similar to  $k_1$  but an additional energy barrier of approximately  $E_{a,2} = 60$  meV (Rauls and Hornekær 2008). Using Arrhenius-like rate constants, this yields the rate constant  $k_2$  as described in equation (2.3), where  $A_H$  denotes the hydrogenation cross section per carbon atom.

$$k_2 = 4 A_H e^{-\frac{E_{a,2}}{kT}} \quad (2.3)$$

A subsequent barrierless hydrogen addition reaction can take place, again with a reaction rate constant  $k_3 = A_H$ . However, a barrierless hydrogen abstraction reaction is also possible with rate  $k_{2,abs} = A_{abs}$ .

For the third hydrogenated state, hydrogen addition can take place at the four remaining outer edge sites via a reaction with a barrier of  $E_{a,4}$ . Hydrogen abstraction is also possible, but now it has a barrier of  $E_{abs,3} = 30$  meV (Rauls and Hornekær 2008), yielding the reaction rate constant:

$$k_{3,abs} = A_{abs} e^{-\frac{E_{abs,3}}{kT}}. \quad (2.4)$$

These processes continue until all the low-barrier outer edge sites are hydrogenated, adding up to a total of 11 extra H atoms. In short, the differential equations governing the model can be described by equation (2.5) and the reaction rate coefficients are given by equations (2.6) and (2.7)

$$\begin{aligned} \frac{\partial}{\partial t} [\text{H}_n \text{Cor}^+] = & k_n [\text{H}_{n-1} \text{Cor}^+] n_{\text{H}} - k_{n,\text{abs}} [\text{H}_n \text{Cor}^+] n_{\text{H}} \\ & - k_{n+1} [\text{H}_n \text{Cor}^+] n_{\text{H}} + n k_{n+1,\text{abs}} [\text{H}_{n+1} \text{Cor}^+] n_{\text{H}}, \quad n = 1, 2, \dots \end{aligned} \quad (2.5)$$

$$k_n = \begin{cases} 4 A_{\text{H}} e^{-\frac{E_{\text{a},n}}{kT}} & \text{when } n \text{ is even} \\ A_{\text{H}} & \text{when } n \text{ is odd} \end{cases} \quad (2.6)$$

$$k_{n,\text{abs}} = \begin{cases} A_{\text{abs}} e^{-\frac{E_{\text{abs},n}}{kT}} & \text{when } n \text{ is even} \\ A_{\text{abs}} & \text{when } n \text{ is odd} \end{cases} \quad (2.7)$$

From the experiments performed by Mennella et al. (2012) we use the relative cross sections  $A_{\text{H}} \approx 20A_{\text{abs}}$ .

We use these equations to construct a numerical model for the hydrogenation of the coronene cation. The model yields the time evolution of the contribution of all hydrogenation states given the hydrogen beam temperature, the relative cross sections for addition and abstraction and the height of the barriers present. A typical result is shown in figure 2.2.

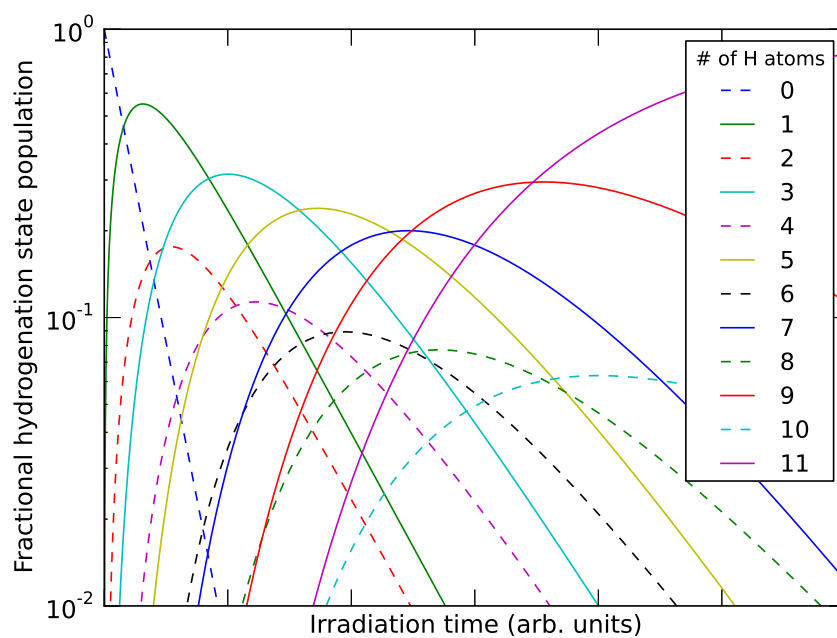


Figure 2.2: Theoretical calculations of the hydrogenation of coronene cations with increasing atomic hydrogen irradiation time. For this model we use the relative addition and abstraction cross sections of Mennella et al. (2012) and we used a hydrogen temperature of 300 K and hydrogenation barriers (if applicable) of  $E_a = 60$  meV.

## CHAPTER 3

### Experimental setup

The experiments are done in an experimental setup named Paultje, which is shown schematically in figure 3. This experimental setup enables us to trap and study molecular ions in the gas phase. These molecular ions are produced chemically in a solution, which is then electrosprayed to bring them into the gas phase.

An ion funnel focusses these ions into a quadrupole ion guide/mass filter before they are electromagnetically trapped in a Paul trap. While being trapped, the ions are bombarded with a mixture of atomic and molecular hydrogen ( $H/H_2$ ), produced by a Slevin-type hydrogen source (Slevin and Stirling 1981).

After the bombardment, an electric field is used to extract the ions from the trap towards a detector with a high time-resolution. If the distance between the trap and the detector is known, we can determine the masses and charges by time-of-flight mass spectrometry, allowing us to determine the contents of the Paul trap.

### 3.1 Electrospray ionisation

Electrospray ionisation, hereafter abbreviated as ESI, is an effective means of bringing large molecular ions into the gas phase. In 2002 J.B. Fenn received the Nobel Prize in Chemistry for establishing ESI as a means of identification and analysis of large biomolecules (Gaskell 1997).

The basic operation principle is to pump the analyte solution through a needle at a high potential into a grounded capillary. The strong electric field resulting from the potential difference permeates the solution and separates the charges in it. The Coulomb repulsion due to the charge accumulation at the needle tip leads to the formation of a Taylor cone. As soon as this

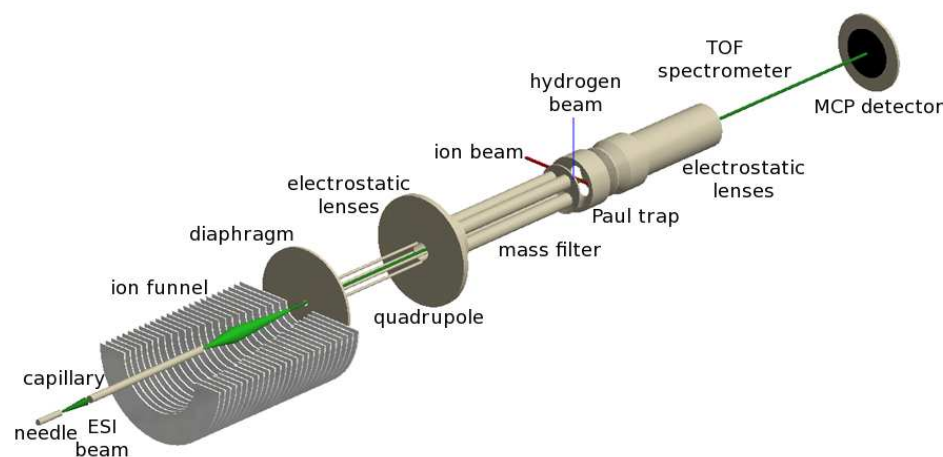


Figure 3.1: A schematic drawing of the Paultje setup at the KVI in Groningen.

electrostatic repulsion overcomes the surface tension of the solution, charged droplets are emitted towards the capillary.

During their flight the solvent evaporates from the droplets, decreasing the droplet size while it retains its charge, hence increasing the surface charge density. When this charge density is high enough, the so-called Rayleigh limit is reached, meaning that the Coulomb repulsion can no longer be compensated by the surface tension of the droplet, causing a fission into smaller droplets.

After this so-called Coulomb explosion, solvent evaporates again from the smaller droplets and the entire process repeats itself until the droplet radius shrinks below 10 nm. At this point the ions evaporate from the droplet directly into the gas phase, while being further accelerated by the electric field.

### 3.2 Ion funnel

After electrospraying, the ions present themselves as a diffuse cloud in a relatively high-pressure environment. Since we eventually want to trap the ions in the Paul trap, we need to focus the cloud into a beam that can be injected into this trap. Also, the performance of the quadrupole mass filter increases significantly when it is applied to a small beam instead of a diffuse cloud.

For this purpose we use an ion funnel, consisting of stacked ring electrodes with decreasing inner diameter. We use an ion funnel instead of a quadrupole ion guide because the ion funnel is very effective at focussing a

diffuse cloud into a narrow beam, whereas a quadrupole device works very well at maintaining this narrow beam (Shaffer et al. 1997).

Two things are necessary for focussing this cloud: a force that drives the ions towards the beam axis and a mechanism to keep them there, i.e. to prevent oscillatory motion with large amplitudes. The former can be easily accomplished with an electromagnetic field that has a corresponding effective potential minimum at the beam axis. This field generally leads to an oscillating trajectory, but at high enough pressures this motion is collisionally damped via interactions with other gas-phase molecules, leading to axial focussing.

In addition to being poor focussing devices for broad beams, quadrupoles are not designed to work at high pressures, contrary to ion funnels. Using an ion funnel has the additional advantage that the device bridges the pressure difference between the electrospray chamber and the high-vacuum quadrupole. An ion funnel consists of a series of equally spaced, axially aligned ring electrodes with decreasing inner radius. A radio-frequency voltage is applied to all rings, and adjacent rings have an equal potential of opposite sign. To understand how this can confine the ion cloud, one can have look at the detailed explanations in Guan and Marshall (1996) and Kelly et al. (2010), a summary of which is provided here.

Let us first look at an ion funnel with ring electrodes of equal inner radius. First we apply a time-varying potential

$$\Phi_0(t) = V_0 \cos \omega t$$

to the ring electrodes, and make sure that the voltages of adjacent electrodes have opposite signs. Setting the inner radius of the ring electrodes at  $r_0$  and the distance between the rings at  $z_0$ , we obtain the potential

$$\Phi(r, z, t) = \Phi_0(t) \frac{I_0(r/z_0)}{I_0(r_0/z_0)} \cos\left(\frac{z}{z_0}\right) \quad (3.1)$$

and the corresponding electric field

$$\begin{aligned} \vec{E}(r, z, t) &= -\vec{\nabla}\Phi(r, z, t) \\ &= \frac{\Phi_0}{z_0} \left( \frac{I_1(r/z_0)}{I_0(r_0/z_0)} \cos\left(\frac{z}{z_0}\right) \hat{r} + \frac{I_0(r/z_0)}{I_0(r_0/z_0)} \sin\left(\frac{z}{z_0}\right) \hat{z} \right), \end{aligned} \quad (3.2)$$

where  $I_0$  and  $I_1$  denote the modified Bessel functions of the zeroth and first order, respectively.  $\hat{r}$  and  $\hat{z}$  indicate the unit vectors in the radial and the axial direction. Separating equation (3.2) into a spatial and a temporal part, we obtain

$$\vec{E}(r, z, t) = \vec{E}_0(r, z) \cos \omega t. \quad (3.3)$$

As a result of the field in equation (3.3), the ion will perform a fast oscillatory motion superimposed on its drift motion. Under the condition

that this driven oscillation is fast compared to the drift motion, the ion experiences the time-averaged rf-field as a static potential, the so-called pseudo-potential (Silveira et al. 2010)

$$V^*(r, z) = \frac{q|E|^2}{4m\omega^2}, \quad (3.4)$$

which can be expanded into

$$V^*(r, z) = \frac{q\Phi_0^2}{4m\omega^2 z_0^2} \frac{1}{I_0^2(r_0/z_0)} \times \left[ I_1^2\left(\frac{r}{z_0}\right) \cos^2\left(\frac{z}{z_0}\right) + I_0^2\left(\frac{r}{z_0}\right) \sin^2\left(\frac{z}{z_0}\right) \right]. \quad (3.5)$$

This potential field clearly drives the ions towards the center of the funnel and additional collisional cooling will confine the ions axially. The initial design with equal ring electrode inner diameter throughout the funnel was improved by letting the inner diameter decrease throughout the ion funnel (Shaffer et al. 1997). Together with a DC voltage gradient along the  $z$ -axis, this allows for ion focussing and converts the initial diffuse ion cloud into a small collimated beam, which is perfectly suitable for a multipole ion guide. These effects are clearly visible in simulations performed by Shaffer et al. (1997).

### 3.3 Ion mass filter

After the passage through the ion funnel, the ions pass through a quadrupole mass filter. This device enables us to select the ions with the exact mass-over-charge ratio that we wish, which is necessary because the electrosprayed solution practically always has contaminants. The quadrupole mass filter allows us to remove these contaminants almost completely. The exact workings of these quadrupoles are described in Paul (1990), but we will summarize the most important aspects here.

Our ion guide consists of four identical, hyperbolically shaped, metal electrodes, arranged concentrically in a circle. Assuming a Cartesian coordinate system, we assign the  $z$ -axis to the (long) axis of our system. We choose our  $x$ - and  $y$ -axis in such a manner that two electrodes are placed symmetrically on the  $x$ -axis and two on the  $y$ -axis. Generally, the electric quadrupole potential is given by

$$\Phi = \frac{\Phi_0}{2r_0^2} (\alpha x^2 + \beta y^2 + \gamma z^2). \quad (3.6)$$

In this specific electrode configuration, we have  $\alpha = -\beta = 1$ ,  $\gamma = 0$  to satisfy the Laplace condition

$$\nabla^2 \Phi = \frac{\Phi_0}{r_0^2} (\alpha + \beta + \gamma) = 0, \quad (3.7)$$

This gives rise to the following electric fields

$$E_x = -\frac{\Phi_0}{r_0^2}x, \quad E_y = \frac{\Phi_0}{r_0^2}y, \quad E_z = 0.$$

For a constant voltage  $\Phi_0 = U$ , this leads to the equations of motion

$$\ddot{x} = -\frac{e}{mr_0^2}Ux, \quad \ddot{y} = \frac{e}{mr_0^2}Uy, \quad \ddot{z} = 0.$$

It can be easily seen from these equations that ions will oscillate in the  $x$ -direction, whereas they will be driven away exponentially in the  $y$ -direction. However, if we apply an additional radio-frequency voltage  $V$  with frequency  $\omega$ , the time-varying potential becomes

$$\Phi_0 = U + V \cos \omega t,$$

leading to the following equations of motion

$$\ddot{x} + \frac{e}{mr_0^2}(U + V \cos \omega t)x = 0, \quad (3.8a)$$

$$\ddot{y} - \frac{e}{mr_0^2}(U + V \cos \omega t)y = 0. \quad (3.8b)$$

After substituting

$$a_u = \frac{4eU}{mr_0^2\omega}, \quad q_u = \frac{2eV}{mr_0^2\omega}, \quad \tau = \frac{\omega t}{2},$$

$$a_x = -a_y = a_u, \quad q_x = -q_y = q_u,$$

we obtain

$$\frac{d^2x}{d\tau^2} + (a_x + 2q_x \cos 2\tau)x = 0, \quad (3.9a)$$

$$\frac{d^2y}{d\tau^2} + (a_y + 2q_y \cos 2\tau)y = 0. \quad (3.9b)$$

These differential equations are second-order Mathieu differential equations in their canonical form. These equations have two types of solutions, stable and unstable, depending on the values of a  $a_u$  and  $q_u$ .

In a stable region of the  $a_u, q_u$ -plane, the Mathieu equation has a stable solution, leading to oscillatory motion. In an unstable region, however, the amplitudes diverge exponentially, so the particles will not be confined.

Since we want to confine the ions in the  $x$ - and  $y$ -direction and both  $a_x, a_y$  and  $q_x, q_y$  have opposite signs,  $a_u$  and  $q_u$  have to be chosen very carefully to lie in stable regions for both spatial dimensions. A part of the stability diagram for a quadrupole is presented in Figure 3.3.

It is possible to define an operation line in such a diagram, with different points on this line corresponding to different masses while keeping  $U$  and  $V$

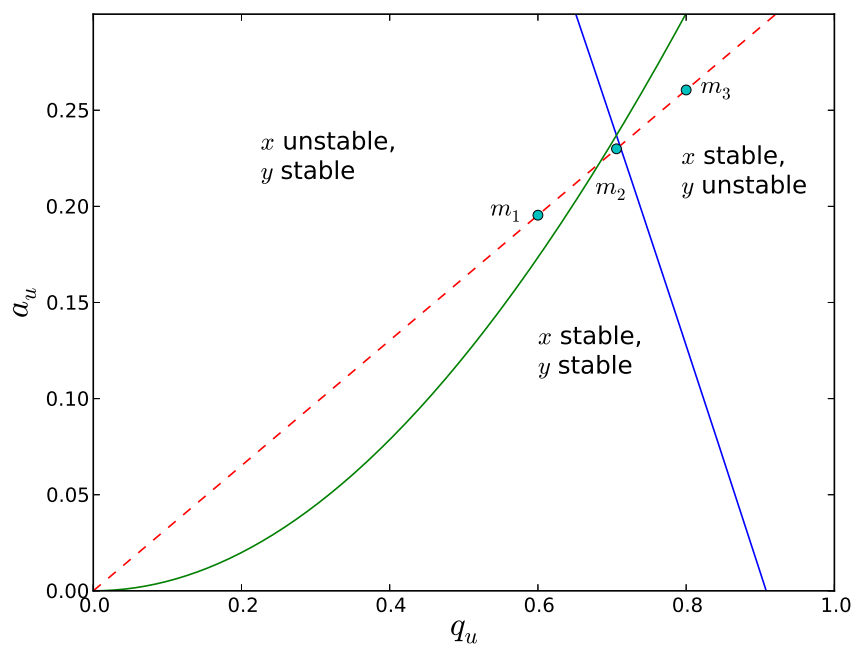


Figure 3.2: The stability diagram for a quadrupole mass filter. The red dashed line represents the operation line on which all the masses lie. Only mass  $m_2$  lies in a stability region and the other masses are filtered out.  $a = 4eU/mr_0^2\omega$ ,  $q = 2eV/mr_0^2\omega$ .

constant. Such an operation line is shown in Figure 3.3. It is clearly visible that only a small part of this operation line lies in a stability region, so only the masses corresponding to the points on the operation line in the stability region are confined. Hence, by carefully selecting the values for  $U$  and  $V$ , it is possible to filter for very specific masses while getting rid of the other masses.

### 3.4 Paul ion trap

After having travelled through the quadrupole ion guide, the ions are inserted into the Paul trap. The Paul trap, named after Wolfgang Paul who received the 1989 Nobel Prize in Physics for its invention, works in a similar manner as the quadrupole ion guide.

Instead of four identical electrodes, one hyperbolically shaped ring electrode and two hyperbolic, rotationally symmetric caps are used. The ring electrode is placed in the  $x, y$ -plane, while the end caps electrodes are placed perpendicular to the  $z$ -axis on both sides of the ring. For this electrode configuration to meet the condition in equation (3.7), we have  $\alpha = \beta = 1$ ,  $\gamma = -2$ , giving rise to an electric field of the form

$$\Phi = \frac{\Phi_0}{2r_0^2} (r^2 - 2z^2) \quad (3.10)$$

where  $r^2 = x^2 + y^2$  represents the radial distance to the  $z$ -axis.

The equations of motion for an ion inside a trap will again resemble the Mathieu differential equations if we apply the voltage  $\Phi_0 = U + V \cos \omega t$  between the ring electrode and the end cap electrodes,

$$\frac{d^2 r}{d\tau^2} + (a_r + 2q_r \cos 2\tau) r = 0, \quad (3.11a)$$

$$\frac{d^2 z}{d\tau^2} + (a_z + 2q_z \cos 2\tau) z = 0. \quad (3.11b)$$

Consequently, using the right values of  $a_u$  and  $q_u$  will lead to oscillatory motion in both the  $r$ - and the  $z$ -direction and thus entrapment of the ions. Although being trapped, the ions still have a kinetic energy of several eV when they enter the trap. To dispose of this energy, helium is injected into the trap as a buffer gas, collisionally cooling the ions to room temperature.

### 3.5 Mass spectrometry

After the Paul trap, the ions are extracted into the Time-Of-Flight (TOF) tube with an electric field  $V_0$ . A micro-channel plate (MCP) is placed at the end of the TOF tube as a detector. Since the initial kinetic energy of

the ions is negligible compared to the potential electric energy, we can state that after the extraction

$$\frac{1}{2}mv^2 = zV_0, \quad (3.12)$$

$$\frac{m}{z} = \frac{2V_0}{v^2}, \quad (3.13)$$

where  $z$  represents the ion charge. Setting the distance between the extraction electrodes and the detector equal to  $d$ , we can derive the time-of-flight  $\tau$  as a function of the mass-over-charge ratio.

$$\tau \left( \frac{m}{z} \right) = d/v = \frac{d}{\sqrt{2V_0}} \sqrt{\frac{m}{z}}. \quad (3.14)$$

After its flight through the TOF tube, the ion reaches the MCP detector. The MCP is a 50 mm diameter silicon plate of typically 2 mm thickness perforated by tubes of approximately 10  $\mu\text{m}$  diameter. These tubes are at a slight angle with respect to the normal, typically around  $8^\circ$ , ensuring that a particle that enters a tube hits one of the walls. Since there is a large electric field applied through the detector, a particle hitting the detector frees some electrons, triggering an avalanche as these electrons subsequently hit the walls of the tube, freeing even more electrons and thus creating a detectable signal at the electrode at the back of the MCP.

### 3.6 Atomic hydrogen source

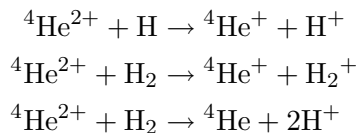
Since we are looking at the sticking of hydrogen atoms to PAHs, we need a device to spray atomic hydrogen at the gaseous PAHs. The device we use is an RF discharge source as described in Slevin and Stirling (1981), consisting of a vacuum pyrex tube inside a metal resonance cavity. There is a helical coil around the pyrex tube which is fed with a radio-frequency signal that resonates inside the metal cavity. This produces a very strong alternating axial magnetic field, leading to the dissociation of the molecules (Toennies et al. 1979) inside the pyrex tube. Before use, the tube is cleaned to remove impurities that enhance recombination and the pyrex tube is cooled with water to reduce recombination even further (Ciric et al. 1985).

We also employ a teflon tube to guide the beam into the trap. This tube is cleaned beforehand with ortho-phosphoric acid to remove impurities that would enhance recombination on the walls. The teflon tube is also cooled via a liquid nitrogen bath to lower the recombination on the wall.

We determine the dissociation fraction of the hydrogen beam with a 40 keV  $^4\text{He}^{2+}$  ion beam produced with an ECR ion source (ECRIS). We cross both beams inside the Paul trap of our setup and as the ion beam collides

with the hydrogen beam, it ionizes both H and H<sub>2</sub> through electron capture. Other processes than electron capture are also taking place, but electron capture is the most dominant process. The interested reader can have a look at Hoekstra (1990) to see their characteristics.

The produced H and H<sub>2</sub> ions are then extracted into the TOF tube to produce a mass spectrum in order to measure the relative amounts of H<sup>+</sup> and H<sub>2</sub><sup>+</sup>



The probability with which these reactions occur is directly proportional to their collisional ionisation cross sections, which are  $\sigma_{21}(\text{H})$ ,  $\sigma_{21}(\text{H}_2)$  and  $\sigma_{20}(\text{H}_2)$  respectively. These cross sections are experimentally determined by Shah and Gilbody (1978) for  ${}^3\text{He}^{2+}$  at energies between 4 and 343 keV. Because the cross section varies with velocity, we use their cross sections for an ion energy of 30 keV, since a 30 keV  ${}^3\text{He}^{2+}$  ion has the same velocity as a 40 keV  ${}^4\text{He}^{2+}$  ion.

If we set the amount of detected H<sup>+</sup> as  $A_{\text{H}^+}$  and the amount of H<sub>2</sub><sup>+</sup> as  $A_{\text{H}_2^+}$ , we find

$$A_{\text{H}^+} = n_{\text{H}}\sigma_{21}(\text{H}) + n_{\text{H}_2}\sigma_{20}(\text{H}_2), \quad (3.15)$$

$$A_{\text{H}_2^+} = n_{\text{H}_2}\sigma_{21}(\text{H}_2). \quad (3.16)$$

Rewriting this into eq. (3.17), it is very straightforward to determine the dissociation fraction from the peak ratios.

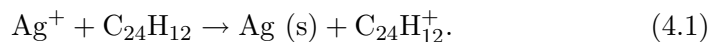
$$\frac{n_{\text{H}}}{n_{\text{H}_2}} = \frac{\sigma_{21}(\text{H}_2)}{\sigma_{21}(\text{H})} \left( \frac{A_{\text{H}^+}}{A_{\text{H}_2^+}} - \frac{\sigma_{20}(\text{H}_2)}{\sigma_{21}(\text{H}_2)} \right) \quad (3.17)$$

From our observed peak ratios, we eventually find  $\frac{n_{\text{H}}}{n_{\text{H}_2}} \approx 0.4$ .

## 4.1 Sample preparation

We are able to produce the coronene cation in a chemical solution. The basis of a sample is 1 mL of an oversaturated solution of coronene in methanol. After centrifuging to remove sediment from the upper layers, a sample of 600  $\mu\text{L}$  saturated coronene solution is obtained without solid residue. The choice of the solvent is crucial in this matter, since it should be able to dissolve both the apolar neutral coronene and its ionized counterpart. For example, hexane is superior to methanol when solely considering dissolving neutral coronene, but as soon as the coronene is ionized, the hexane is not sufficient anymore, since it lacks the polarity (asymmetric internal charge distribution) to dissociate the ionic bonds. The opposite is true for water. As a very polar molecule, it cannot dissolve neutral coronene and hence does not suffice as a solvent for the experiment. For the purpose of ionizing coronene in solution, methanol turns out to be the Aristotelian golden mean, as it dissolves both neutral and ionized coronene.

We create the coronene cation based on the procedure as described in Maziarz (2005). Starting from 600  $\mu\text{L}$  saturated coronene solution, we add 50  $\mu\text{L}$  of a 10 mM solution of  $\text{AgNO}_3$  in 50:50 methanol:ethanol. An additional 350  $\mu\text{L}$  methanol ensures a sample volume of 1 mL. With 7.29 eV, coronene has a slightly lower ionization energy (Lias 2005) than silver (7.58 eV, Loock et al. (1999)) and therefore the  $\text{Ag}^+$ -ion transfers its charge to the neutral coronene. The newly formed coronene cation remains dissolved, while the neutral silver precipitates from the solution as a solid, making the reaction irreversible:



## 4.2 Operational procedure

The mass spectra shown in chapter 5 are the average of typically 100 individual measurements. These individual measurements are all controlled and performed by software written in LabView, and this software operates in experimental cycles. Each individual measurement is represented by one cycle, which consists of the following operations:

1. Inject electrosprayed ions into the Paul trap. This phase lasts typically for 0.4 seconds.
2. Simultaneously, helium buffer gas is pumped into the trap to cool the ions collisionally. This improves the trapping significantly. This buffer gas phase lasts just as long as the trap loading phase.
3. The ions are now kept trapped in the Paul trap. At the same time, the hydrogen source is irradiating the trap contents with a beam of atomic hydrogen.
4. After a predetermined amount of time, the trap contents are ejected into the time of flight tube. Having the same kinetic energy, the heavier ions will fly slower and thus reach the detector at the end at a later time. This allows us to perform mass spectrometry of the trap contents.

Since the setup is not designed for trapping molecules for longer than a few seconds, problems start to arise for irradiation times exceeding 5 seconds.

First of all, the signal suffers from trap losses. These losses emanate from the fact that the energy distribution always contains the high-energy tail that can escape from the trap. Another problem is that coronene cations and their hydrogenated counterparts may at some time have their charge removed during a reaction. Being free of charge, these molecules do not feel the electromagnetic field anymore and are therefore no longer trapped.

The second problem is due to the helium buffer gas. As soon as the helium valve is closed after the trap loading is finished, pressure is building up inside the helium tube. If this pressure becomes too high when the next cycle begins, the pressure in the entire setup will become too high and certain sensitive parts, such as the detector, might be damaged. It is therefore crucial that the pressure build-up is mitigated by a mass flow controller between the helium bottle and the buffer tube that ends inside the trap.

The tuning of the present mass flow controller is too coarse to allow for a sufficiently slow pressure build-up for irradiation times longer than 5 seconds. We work around this problem by venting the helium tube multiple times during one cycle when we wanted to irradiate longer than 5 seconds.

It remains unclear whether this affects the simultaneous hydrogenation process, so we decide not to use those measurements for quantitative analysis. However, a qualitative look at the spectra of those measurements already provides us with a lot of insight.

## 5.1 Raw data

The raw data obtained from a measurement is a time-of-flight spectrum with a time resolution of 1 ns and a total duration of 50  $\mu$ s. This is sufficient to detect particles with masses between 1 and 950 amu. To increase the signal-to-noise ratio, this spectrum is actually the average of a series of identical measurements, where one series typically consists of 100 individual measurements. With the right calibration, one can convert these time-of-flight spectra to mass spectra using equation (5.1),

$$\frac{m}{z}(\tau) = \left( \frac{\tau - b}{m_0} \right)^2. \quad (5.1)$$

We perform measurements for irradiation times between 1 and 5 seconds and two additional long exposures of 15 and 30 seconds. The mass spectra of the short exposures are shown in figure 5.1 and the long exposures are shown in figure 5.2.

Each mass in the spectrum is accounted for by a gaussian peak with a width that corresponds to the mass resolution at that mass. This finite mass resolution is caused by thermal dispersion and initial displacement of the ions and has a value of  $\frac{m}{\Delta m} \approx 200$ . Since the mass of the singly charged coronene cation is 300 amu, peaks around this mass have FWHM  $\approx 1.5$ . It is therefore difficult to distinguish one hydrogenation state from the next, because their mass peaks will be blended. Luckily, their widths will be identical, so the best way to extract all mass peaks from the mass spectrum is by fitting multiple Gaussians with an identical fixed width.

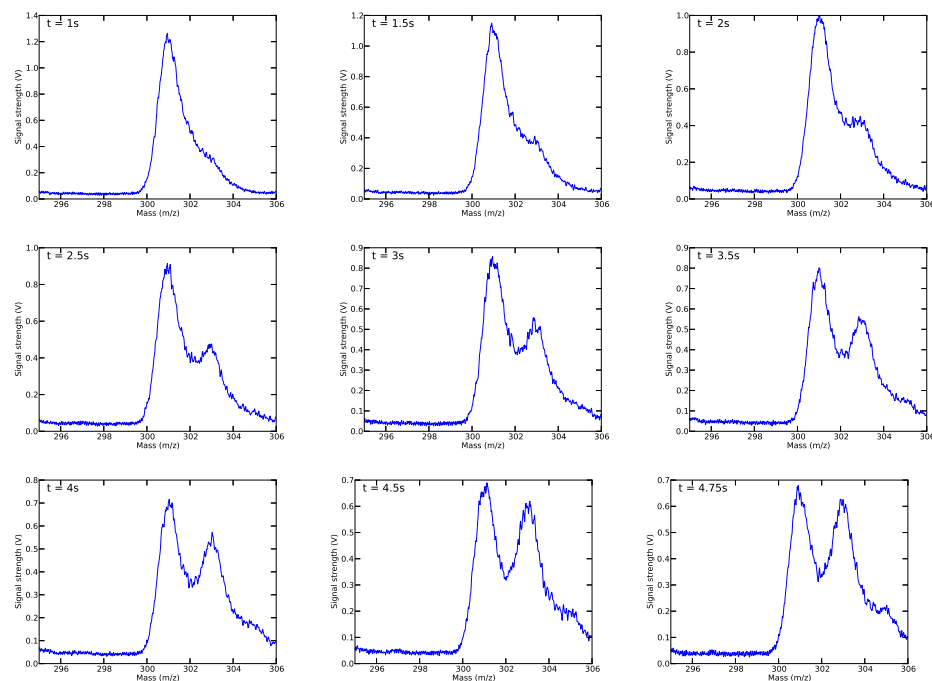


Figure 5.1: Evolution of the coronene cation mass spectrum with increasing H irradiation time. For larger versions of these plots, see appendix A.

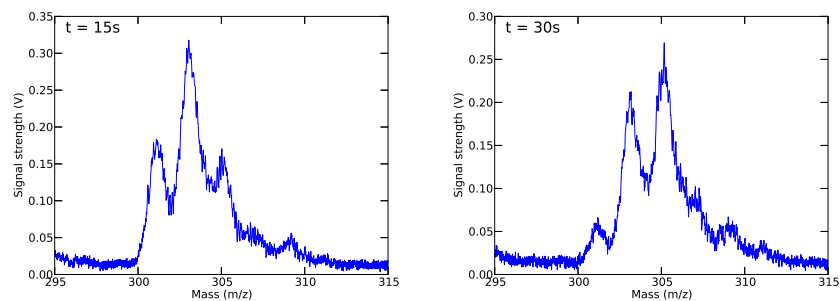


Figure 5.2: Mass spectra taken after exposing coronene cations to hydrogen for 15 and 30 seconds.

## 5.2 Observed trends

A mass spectrum of coronene without hydrogen irradiation is shown in figure A.1. It has a clear peak at a mass of 300, which matches the mass of a coronene molecule exactly.

As we start irradiating, we see that the peak at 300 disappears and that a peak at  $m/z = 301$  appears. We also observe an emerging peak at a mass of 303 that grows more dominant with irradiation time and for higher irradiation times there is even a peak at  $m/z = 305$  visible.

Comparing the spectra for different H irradiation times, there are two things clearly visible. First of all, the only visible peaks are at odd hydrogenation states, e.g. at  $\frac{m}{z} = 301, 303$ , etc. If there is any signal from the even hydrogenation states, it is not visible by eye, because the surrounding odd hydrogenation states overwhelm it completely with their Gaussian wings. Although not visible by eye, we can still determine the contribution of the even states. This contribution is relatively small, but it is still measurable.

The second thing that is clearly visible in the spectra is the shift to higher masses with increasing H irradiation time. This indicates that hydrogenation increases with H irradiation time, as is especially clear from the long exposure spectra.

The raw mass spectra give us a rough indication of the hydrogenation process, but we need a more quantitative understanding of the process. We therefore analyze the short exposure data with a model that accounts for the addition of up to 12 hydrogen atoms.

Every hydrogenation state is represented by a gaussian with a fixed width that corresponds to the resolution of the mass spectrometer, as shown in equation (6.1). Because of this fixed width, the amount of coronene molecules in a certain hydrogenation state is measured directly by the amplitude of the corresponding gaussian. An additional advantage is that the even hydrogenation states can be measured as well, although they remain more or less hidden in the gaussian wings of the odd states.

There is also a baseline present in the mass spectra. This baseline is uniform throughout the spectral region of interest and can therefore be included easily in the model as the additional constant  $C$ . The model can then be summarized as:

$$y = C + \sum_{i=0}^{11} A_i \exp \left[ -\frac{(x - m_{300+i})^2}{2\sigma^2} \right], \quad (6.1)$$

where  $\sigma$  denotes the standard deviation of the Gaussian peaks that corresponds to the resolution of the mass spectrometer.

## 6.1 Line evolution

The technique described above allows us to study the time evolution of each separate hydrogenation state individually. We show this evolution for the first five hydrogenation states in figure 6.2. In this figure we see that within a second there are no more bare cations left and that the relative abundance

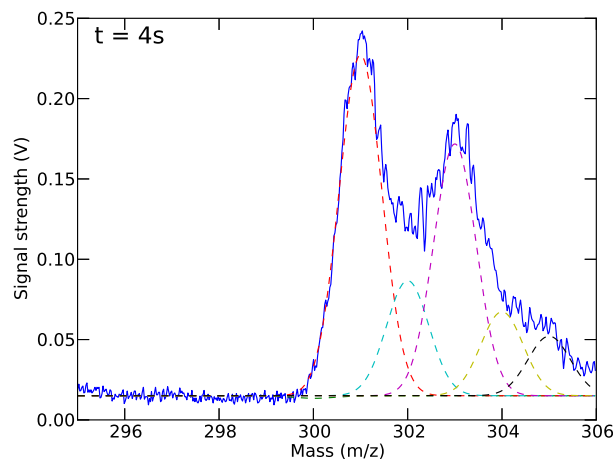


Figure 6.1: Fixed width gaussian analysis of the mass spectrum obtained after irradiating coronene cations with atomic hydrogen for 4 seconds.

of the first hydrogenation state already starts to decrease with time. This clearly indicates that almost instantaneously all the coronene is in the first hydrogenation state and starts to hydrogenate further. This observation fits the earlier prediction that the first hydrogenation is barrierless perfectly.

Furthermore we see that the second hydrogenation state,  $n_{\text{CorH}_2^+}$ , decreases with time in a fashion similar to the first hydrogenation state. This can be explained by the fact that the production of this state out of the first hydrogenation state is impeded by a barrier. At the same time,  $n_{\text{CorH}_2^+}$  is hydrogenated without a barrier, so this process happens a lot faster. Therefore, the amount of  $n_{\text{CorH}_2^+}$  is limited by the speed of its formation process, which is in turn limited by the amount of ions in the first hydrogenation state. Since the latter is decreasing with time, so is the amount of ions in the second hydrogenation state. The third, fourth and fifth hydrogenation are all increasing with irradiation time. This is as expected, since most ions are still in the first hydrogenation state after 1 second.

If we compare the results from figure 6.2 with the model for the hydrogenation from section 2.2, we see that we are still in the early stages of hydrogenation. In figures 6.3 to 6.5 we zoom in on this phase and we compare models with different values for the relative abstraction cross section. From these figures we see that abstraction does not play a significant role at short irradiation times. This justifies the neglect of abstraction when the hydrogenation barriers are derived, which simplifies the mathematics significantly.

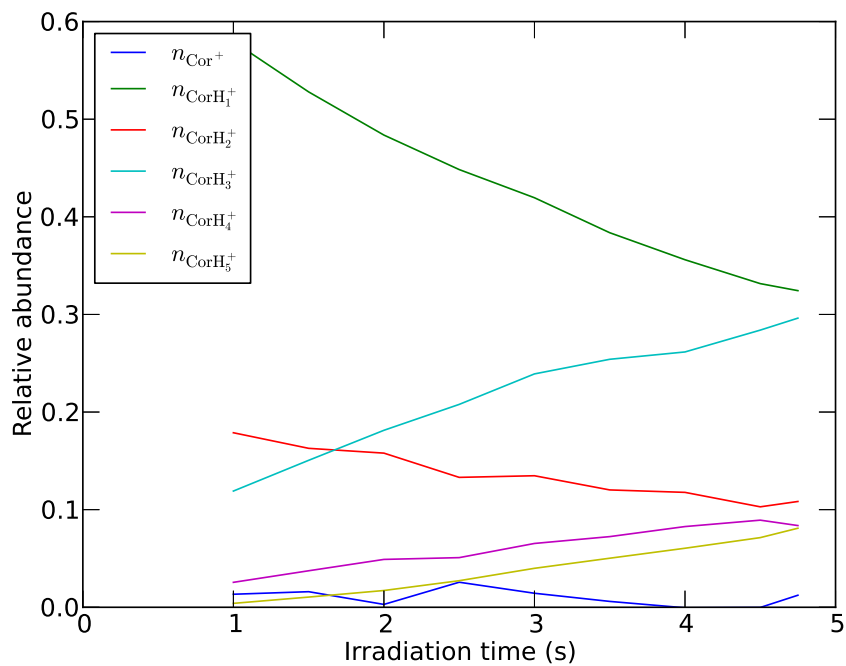


Figure 6.2: The time evolution of the first five hydrogenation states.

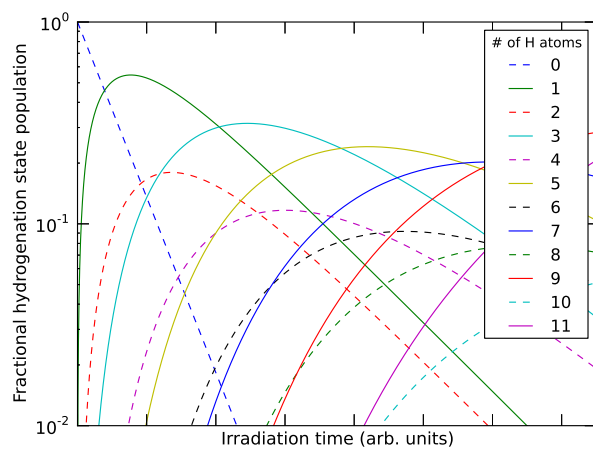


Figure 6.3: The model from section 2.2, but without abstraction.

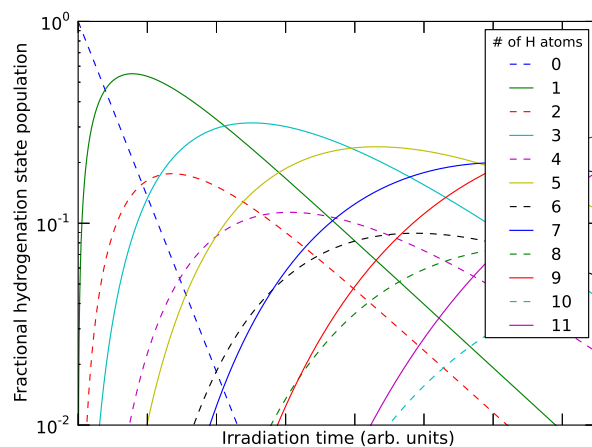


Figure 6.4: The model from section 2.2 with a relative abstraction cross section from Mennella et al. (2012).

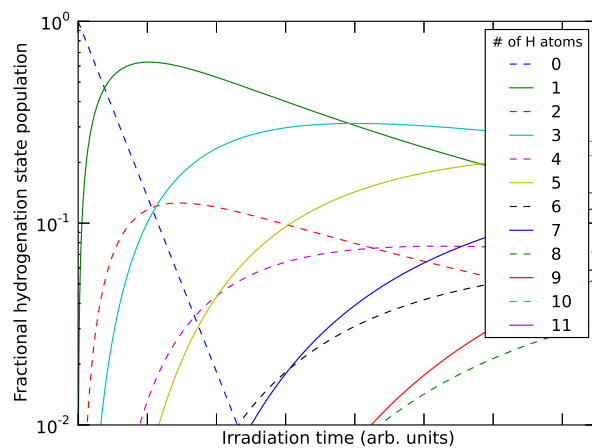


Figure 6.5: The model from section 2.2 with an abstraction cross section equal to the cross section for hydrogenation.

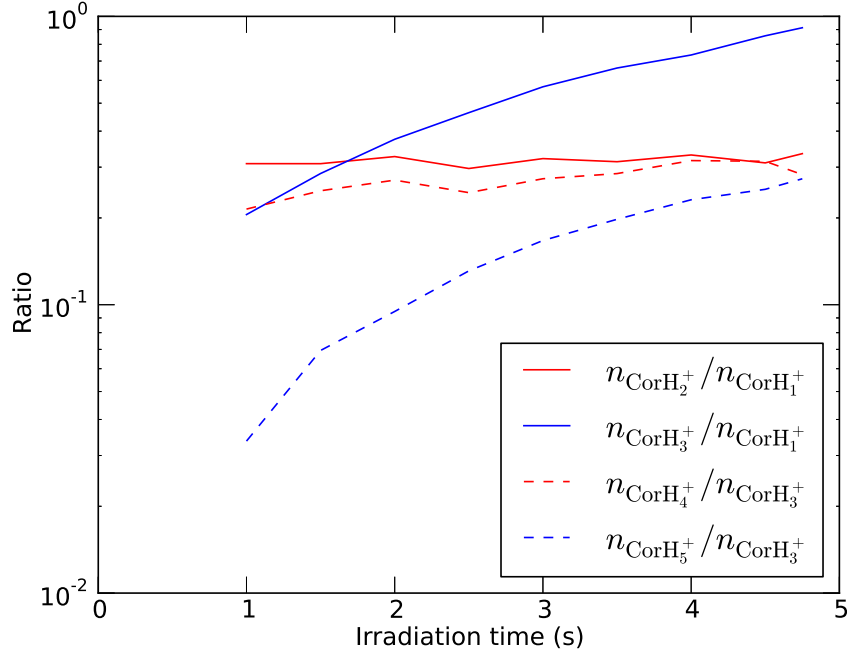


Figure 6.6: Measured ratios of hydrogenation states.

## 6.2 Deriving energy barriers

### The first barrier

One of the striking resemblances between theory and experiment is the constant ratio of the contributions from the first and the second hydrogenation state ( $\text{CorH}^+$  and  $\text{CorH}_2^+$ ). This is very clear from figures 6.3 to 6.6. We can therefore use equation (6.2) to obtain the height of the first barrier.

$$\frac{d}{dt} \left( \frac{n_{\text{CorH}_2^+}}{n_{\text{CorH}^+}} \right) = \frac{n_{\text{CorH}^+}(t)n'_{\text{CorH}_2^+}(t) - n_{\text{CorH}_2^+}(t)n'_{\text{CorH}^+}(t)}{n_{\text{CorH}^+}^2(t)} = 0 \quad (6.2)$$

Recalling the equations from section 2.2, we get the following expressions for the temporal derivatives of  $\text{CorH}^+$  and  $\text{CorH}_2^+$ :

$$\frac{d n_{\text{CorH}^+}}{dt} = -A_1 e^{-\frac{E_a}{k_B T}} n_{\text{CorH}^+} n_H, \quad (6.3)$$

$$\frac{d n_{\text{CorH}_2^+}}{dt} = A_1 e^{-\frac{E_a}{k_B T}} n_{\text{CorH}^+} - A_2 n_{\text{CorH}_2^+} n_H. \quad (6.4)$$

Combining equations (6.2), (6.3) and (6.4), we get the following expression:

$$\left(1 + \frac{n_{\text{CorH}_2^+}}{n_{\text{CorH}^+}}\right) A_1 e^{-\frac{E_a}{k_B T}} - A_2 \frac{n_{\text{CorH}_2^+}}{n_{\text{CorH}^+}} = 0. \quad (6.5)$$

This can be rewritten in an expression for the energy barrier, as shown in equation (6.6). We can apply this equation to all our data points, because the basic assumption that the ratio of  $\text{CorH}^+$  and  $\text{CorH}_2^+$  is constant is valid throughout our entire measurement sequence. This yields a very constant value for the energy barrier of approximately 72 meV, as can be seen in figure 6.7:

$$E_2 = -k_B T \ln \left( \frac{A_2}{A_1} \frac{1}{1 + \frac{n_{\text{CorH}^+}}{n_{\text{CorH}_2^+}}} \right). \quad (6.6)$$

### The second barrier

The second hydrogenation barrier is encountered by the fourth hydrogen atom that tries to bind to the hydrogenated coronene cation, so we will refer to it as  $E_4$ . Similarly to the first barrier, we observe that for this hydrogenation step the ratio  $n_{\text{CorH}_4^+}/n_{\text{CorH}_3^+}$  is more or less constant. Again assuming that abstraction is negligible, we can derive this barrier in a similar fashion as we did for the first one, which yields the expression in equation (6.7):

$$E_4 = -k_B T \ln \left( \frac{A_4 + \frac{n_{\text{CorH}_2^+}}{n_{\text{CorH}_3^+}} A_2}{A_3} \frac{1}{\frac{n_{\text{CorH}_3^+}}{n_{\text{CorH}_4^+}} + 1} \right). \quad (6.7)$$

Using this expression, we obtain the barrier for all measurements, as shown in figure 6.7. For the calculation of the second barrier, we ignore the data points with an irradiation time of 2 seconds and shorter. At that time, the peaks of  $n_{\text{CorH}_3^+}$  and  $n_{\text{CorH}_4^+}$  are still too low to be detected with sufficient accuracy. Additionally, at short irradiation times, these two peaks have not reached an equilibrium state yet, which can also be seen in figure 2.2. Taking these conditions into account, we find a barrier height of  $E_4 = 43$  meV.

This fourth hydrogenation on the coronene cation is electronically equivalent to the third hydrogenation on a neutral coronene molecule. Rauls and Hornekær (2008) predict that the third hydrogenation to an outer edge carbon atom has an associated barrier of 40 meV, which is very close to the barrier height we find experimentally for the fourth hydrogenation of the

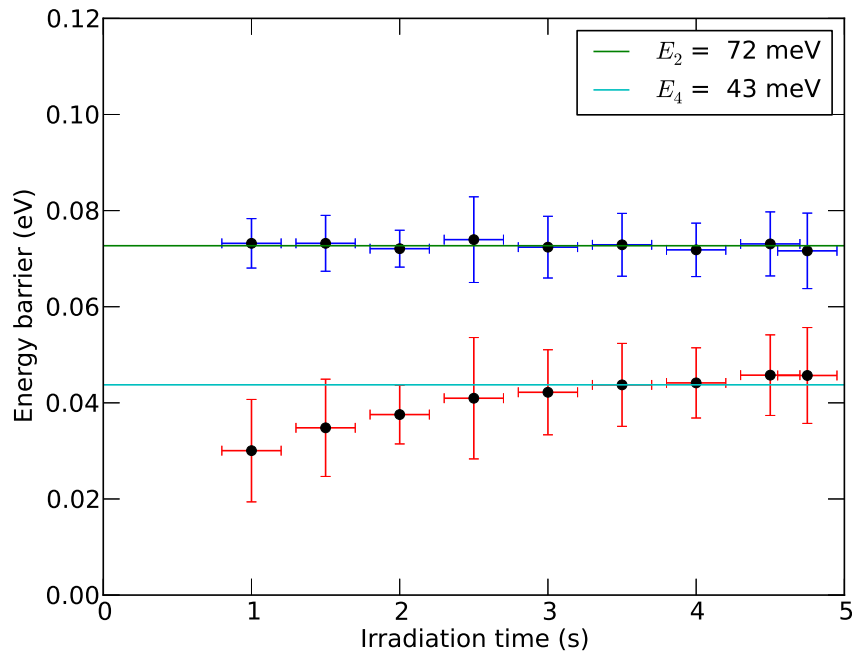


Figure 6.7: The first and the second barrier as obtained from the mass spectra. In calculating the average value for  $E_4$ , we ignore the first three data points with an irradiation time below 2 s. The errors along the time axis originate from the finite Paul trap loading time.

cation.

In figure 6.7 we show the estimated value of  $E_2$  and  $E_4$  at each irradiation time. For the first barrier all the values agree with each other very well. In the second barrier we observe that for the shortest irradiation times the barrier height appears to increase with time. This is probably due to the fact that for short irradiation times the third and fourth hydrogenation state are not in equilibrium yet. We therefore ignore the measurements with irradiation times shorter than 2 s for the calculation of the second barrier.

The errorbars shown in figure 6.7 include only errors from fitting the gaussian model to the experimental data. Other factors are not included in these errorbars.

## 7.1 Summary

We irradiate coronene cations with a beam of atomic hydrogen and measure a mass spectrum of the irradiation products. After varying the irradiation time from 1 second up to 30 seconds, we find that the measured masses increase with irradiation time. We also observe that the mass spectra are dominated by the coronene cations with an odd number of hydrogen atoms. This indicates that the hydrogenation of the coronene cation is subject to a barrier at every second hydrogen atom addition. The first two barriers can be measured using models for chemical kinetics featuring Arrhenius statistics and are determined at a value of  $72 \pm 6$  meV and  $40 \pm 10$  meV.

The dominance of odd hydrogenation states is shown to continue until high hydrogenation states. This indicates that the barrier for every second hydrogenation also exists for these higher hydrogenation states.

## 7.2 Comparison with previous work

Hydrogenation of PAHs has been studied by Mennella et al. (2012), who look at the changing IR spectrum of coronene films during irradiation with an atomic deuterium beam. They find clear evidence of hydrogenation and subsequent abstraction and derive cross sections for these processes. The coronene hydrogenation cross section they obtain has a value of  $1.1 \text{ \AA}^2$  and for abstraction a cross section of  $0.06 \text{ \AA}^2$  is found. This abstraction cross section shows that hydrogenated PAHs are efficient at forming  $\text{H}_2$  in the ISM.

Other studies are able to derive rate constants for the first addition of hydrogen, oxygen and nitrogen atoms to cations of several PAHs (Betts et al. 2006; Snow et al. 1998; Mennella et al. 2012).

We compare the experimental results of the coronene cation with the calculations for the neutral coronene molecule from Rauls and Hornekær (2008). For the first few hydrogen additions, the barriers derived from our experiment are consistent with those predicted from the calculation for the neutral coronene molecule. We are able to calculate the barriers of the second and the fourth hydrogen sticking, and compare them to the calculations of Rauls and Hornekær (2008). Considering that the second hydrogenation of the coronene cation is electronically equivalent to the first hydrogenation of the neutral molecule, the calculated barriers (60 and 40 meV) are similar to those derived from the experimental data (72 and 40 meV). This shows that at least for the first hydrogenations the coronene cation behaves in a fashion similar to the predictions for the hydrogenation of the neutral molecule.

While for the first hydrogenation the agreement between the neutral calculations and the cation experiment is rather stunning, our results start to diverge for the subsequent hydrogenations. Rauls and Hornekær (2008) predict that after the fourth hydrogenation the barrier vanishes, while we observe alternating barriers beyond the fourth hydrogenation. Rauls and Hornekær (2008) include a hydrogen atom sticking to an edge carbon atom in their calculations (see figure 1.2), which might change the course of the subsequent hydrogenations. According to their calculations this is the favorable path to follow, because it has the lowest reaction barrier.

The work by Rauls and Hornekær (2008) has been followed by Thrower et al. (2012) to study the hydrogenation of neutral PAHs experimentally. They irradiate solid phase coronene films with a 2000 K atomic deuterium beam. After this irradiation, they gradually increase the film temperature and simultaneously monitor the evaporating species with mass spectrometry. Their data shows that all hydrogenation states are equally populated without a preference for the odd hydrogenation states. However, in their experiment they use a hydrogen atom beam of 2000 K. A temperature of 2000 K corresponds to an energy of approximately 170 meV, which is more than enough to overcome possibly existing hydrogenation barriers. Therefore, their reaction rate for hydrogenation with a barrier does not differ that much from unobstructed hydrogenation, hence the invisibility of the hydrogenation barriers.

In summary, while we see that the coronene cation behaves similarly to its neutral counterpart, we also observe that for higher hydrogenation states theoretical predictions and our experimental data diverge.

### 7.3 Consequences for H<sub>2</sub> formation

This research project is carried out to better understand the role of PAHs in the formation of H<sub>2</sub>. Especially superhydrogenated PAHs can enhance the H<sub>2</sub> formation rate through Eley-Rideal reactions with incoming H atoms from the gas phase. These superhydrogenated PAHs are produced by the addition of H atoms to the fully aromatic PAH.

We show that this hydrogenation process can happen for coronene cations in contact with hydrogen atoms at room temperature. The kinetic behaviour of this process matches the theoretical predictions for the neutral coronene molecule. Given that neutral coronene plays a role in the H<sub>2</sub>-formation process, coronene cations should fulfill a similar role in the chemical reaction network.

Molecular hydrogen is also present in clouds subject to an external UV field, the so-called PDRs. This external UV field dissociates H<sub>2</sub> but the fact that it is still found in PDRs indicates that it is shielded from this UV field at higher visual extinction  $A_V$ .

Generally, PAH cations dominate over their neutral counterparts in low UV ( $G_0 \leq 100$ ) PDRs at low visual extinctions ( $A_V < 2$ , Cox and Spaans (2006)), implying that PAH catalyzed H<sub>2</sub> formation can already take place at low  $A_V$ . This increases the region of a cloud where H<sub>2</sub> formation is possible.

From our results we can also derive that reaction rate coefficients are not valid for the entire temperature regime of the ISM. In regions where hydrogenation of PAH cations plays a role, the temperature is typically lower than the energy of the barrier associated with this addition, resulting in a strong temperature dependence of the reaction rate constants.

### 7.4 Outlook

To derive reaction rate constants that are valid throughout the entire applicable temperature regime, we will derive individual cross sections for hydrogenations. We will also combine our model with future experiments to determine the subsequent hydrogenation barriers. This can then be combined to obtain a temperature-dependent reaction rate coefficient for every hydrogenation step. In this manner the chemical models for the H<sub>2</sub> formation in the ISM will be improved significantly.

Ideally, the experiments performed for this project would be repeated with even larger PAHs, such as circumcoronene (C<sub>54</sub>H<sub>18</sub>). This would enable us to check the dependence of the barrier height on the size of the PAH and therefore to assess how H<sub>2</sub> formation depends on the size of the PAH. Combining this knowledge with astronomical PAH size distributions would allow the derivation of actual H<sub>2</sub> formation rates, which can be compared

to astronomical observations and used in numerical models.

Future experiments will include the addition of oxygen atoms to PAHs. This will provide a better knowledge about the formation of small oxygen-containing species, such as the OH radical and the water molecule. These small molecules open up a plethora of chemical pathways and understanding the influence of PAHs on their formation would vastly improve our knowledge about the chemical processes in the ISM as well as the thermal balance, which are all of influence on star formation.

Another region of interest is the influence of hydrogenation on the IR spectrum of PAHs since the presence of PAHs is generally inferred from their IR band emission. Knowing whether and how hydrogenation modifies this emission might allow us to provide better estimates of the amount of PAH molecules present. It might even give us a tool to estimate the amount of hydrogenation of the PAHs present.

In this study we show experimental evidence for the existence of barriers to hydrogenate coronene cations. These barriers present alternating behaviour up to the eleventh hydrogenation. We show that only every second hydrogenation is associated with a barrier and measure the height of the first two barriers to be  $E_2 = 72 \pm 6$  meV and  $E_4 = 40 \pm 10$  meV.

These barrier heights match the theoretical predictions for the electronically equivalent reactions on the neutral coronene molecule. This indicates that cationic PAHs should contribute to the same extent to the formation of molecular hydrogen as their neutral counterparts.

These barriers also imply a strong temperature dependence of the PAH-catalyzed H<sub>2</sub>-formation rate, since these reaction barriers are generally higher than the temperature at which these reactions take place. One simple reaction rate constant will therefore not suffice to successfully model these reactions in the ISM. In a future work we will derive individual cross sections to obtain temperature dependent reaction rates. To make these studies even more encompassing, it is desirable to repeat these measurements with PAHs of a larger size than coronene, such as circumcoronene. This will allow us to study the dependency of the reaction rates on the size of the PAH.

We envisage future experiments to study the addition of oxygen atoms to PAHs as well as the modification of the IR spectrum of PAHs when they become hydrogenated.

## CHAPTER 9

### Acknowledgements

As the old saying goes, no man is an island. During this project I have had a lot of support and help from more than a few people. First of all I would like to thank my supervisors at the Kapteyn institute, Stéphanie Cazaux and Marco Spaans. Stéphanie, you always had confidence in my abilities, even at moments when I did not anymore, and it was probably your incessant encouragement that kept me going in those cases. Thanks a lot for this, I always find it fun discussing science (and non-science) with you and I am really looking forward to four more years of collaboration with you. Marco, many thanks for your support during the last year. Although being a theorist at heart, you were really interested in the experimental part of this project as well, something I really appreciate. What I found most remarkable is that you always made it seem that your advice was just my own idea, and that you had just helped me discover it.

Furthermore I would like to thank the people from the ISM group at the Kapteyn for their constructive feedback throughout the year.

My special thanks goes out to the people of the Atomic and Molecular Physics group at the KVI, where the experiments of this project were performed. You really helped me a lot getting the experiments to work and I enjoyed the time in the laboratory greatly. The beamtimes we had in Berlin and Lund were fantastic experiences and I am really looking forward to the next experiments.

Ronnie, I would like to thank you for your good advice throughout the entire year and I am looking forward to making coffee for four more years.

Thomas, it is because of you and your energetic behaviour that I am now more and more living by the creed of an experimental physicist, “just do it and hope that nature is kind”.

Erwin Bodewits taught me many things during my year as his officemate, among which is the second most important rule of experimental physics: “boring is good, it means that everything is working”. I am afraid I have bit more trouble getting used to that one.

Geert, many thanks for your help and assistance during last year. I really enjoyed working in the lab with you and your jokes made the sometimes long hours worthwhile. Also the trips we made were very cool, although I would recommend you to wear glasses the next time we pass some Danish toll booths.

Olmo, thank you for your helping me in getting familiar with the setup, it really sped up my work in the laboratory. Ina, I would like to thank you for teaching me to alleviate my experimental stress on punching bags rather than concrete walls, although it would have been better if you taught me that a bit earlier.

I would also like to thank the people from the mechanical workshop at the KVI, who were never too busy to help me with many of the practical problems I encountered. They were often able to replace my well-thought, complex solution with an easier, better-working one.

Essential help was also provided by the electronic workshop and the vacuum support group.

The supporting staff at both the KVI and the Kapteyn have always helped me with all the tiny little problems I encountered, for which I would like to thank them.

My gratitude goes out to all my fellow (PhD) students at both the Kapteyn and the KVI, who were always eager to provide me with the necessary distraction and coffee when I needed it the most.

Finally, I would like to thank my family, and my parents in particular. It must have been strange, seeing your son quitting chemistry with the announcement that he will never do chemistry or work in a lab again, only to see him growing up to become an experimental astrochemist. Nevertheless, I really thank you for your never-ending support during all those years.

## BIBLIOGRAPHY

- Bauschlicher, Jr., C. W. (1998). The Reaction of Polycyclic Aromatic Hydrocarbon Cations with Hydrogen Atoms: The Astrophysical Implications. *The Astrophysical Journal, Letters*, 509:L125–L127.
- Betts, N. B., Stepanovic, M., Snow, T. P., and Bierbaum, V. M. (2006). Gas-Phase Study of Coronene Cation Reactivity of Interstellar Relevance. *The Astrophysical Journal, Letters*, 651:L129–L131.
- Cazaux, S. M. (2004). *Grain Surface Chemistry in Astrophysical Objects: From H<sub>2</sub> to complex molecules*. PhD thesis, Kapteyn Astronomical Institute.
- Ciric, D., Dijkkamp, D., Vlieg, E., and de Heer, F. (1985). Selective electron capture into He II (n, l) subshells in collisions of He 2+ with atomic and molecular hydrogen. *Journal of Physics B: Atomic and Molecular Physics*, 18(24):4745.
- Cox, N. L. J. and Spaans, M. (2006). The effects of metallicity, radiation field and dust extinction on the charge state of PAHs in diffuse clouds: implications for the DIB carrier. *Astronomy & Astrophysics*, 451:973–980.
- Gaskell, S. (1997). Electrospray: Principles and Practice. *Journal of Mass Spectrometry*, 32:677–688.
- Gould, R. J. and Salpeter, E. E. (1963). The Interstellar Abundance of the Hydrogen Molecule. I. Basic Processes. *The Astrophysical Journal*, 138:393.
- Guan, S. and Marshall, A. G. (1996). Stacked-ring electrostatic ion guide. *Journal of the American Society for Mass Spectrometry*, 7(1):101–106.
- Hoekstra, R. (1990). *Photons Shedding Light on Electron Capture by Highly Charged Ions*. PhD thesis, Rijksuniversiteit Groningen.

- Kelly, R. T., Tolmachev, A. V., Page, J. S., Tang, K., and Smith, R. D. (2010). The ion funnel: Theory, implementations, and applications. *Mass Spectrometry Reviews*, 29(2):294–312.
- Lias, S. (2005). Ionization Energy Evaluation. In Linstrom, P. and Mallard, W., editors, *NIST Chemistry WebBook, NIST Standard Reference Database Number 69*. National Institute of Standards and Technology, Gaithersburg MD, 20899.
- Loock, H.-P., Beaty, L., and Simard, B. (1999). Reassessment of the first ionization potentials of copper, silver, and gold. *Physical Review A (Atomic, Molecular, and Optical Physics)*, 59:873–875.
- Maziarz, E. (2005). Electrospray ionization Fourier transform mass spectrometry of polycyclic aromatic hydrocarbons using silver(I)-mediated ionization. *Canadian Journal of Chemistry - Revue Canadienne de Chimie*, 85(11):1871–1877.
- Meijerink, R. and Spaans, M. (2005). Diagnostics of irradiated gas in galaxy nuclei. I. A far-ultraviolet and X-ray dominated region code. *Astronomy & Astrophysics*, 436:397–409.
- Mennella, V., Hornekær, L., Thrower, J., and Accolla, M. (2012). The Catalytic Role of Coronene for Molecular Hydrogen Formation. *The Astrophysical Journal, Letters*, 745:L2.
- Norman, C. A. and Spaans, M. (1997). Molecules at High Redshift: The Evolution of the Cool Phase of Protogalactic Disks. *The Astrophysical Journal*, 480:145.
- Oort, J. H. and van de Hulst, H. C. (1946). Gas and smoke in interstellar space. *Bulletin of the Astronomical Institutes of the Netherlands*, 10:187.
- Paul, W. (1990). Electromagnetic Traps for Charged and Neutral Particles. *Reviews of Modern Physics*, 62(3):531–540.
- Rauls, E. and Hornekær, L. (2008). Catalyzed Routes to Molecular Hydrogen Formation and Hydrogen Addition Reactions on Neutral Polycyclic Aromatic Hydrocarbons under Interstellar Conditions. *The Astrophysical Journal*, 679:531–536.
- Shaffer, S. A., Tang, K., Anderson, G. A., Prior, D. C., Udseth, H. R., and Smith, R. D. (1997). A novel ion funnel for focusing ions at elevated pressure using electrospray ionization mass spectrometry. *Rapid Communications in Mass Spectrometry*, 11(16):1813–1817.
- Shah, M. B. and Gilbody, H. B. (1978). Electron capture and  $\text{He}^+(2s)$  formation in fast  $\text{He}^{2+}$ -H and  $\text{He}^+$ -H collisions. *Journal of Physics B Atomic Molecular Physics*, 11:121–131.

- Silveira, J. A., Gamage, C. M., Blase, R. C., and Russell, D. H. (2010). Gas-phase ion dynamics in a periodic-focusing DC ion guide. *International Journal of Mass Spectrometry*, 296(13):36–42.
- Slevin, J. and Stirling, W. (1981). Radio frequency atomic hydrogen beam source. *Review of Scientific Instruments*, 52(11):1780–1782.
- Snow, T. P., Le Page, V., Keheyan, Y., and Bierbaum, V. M. (1998). The interstellar chemistry of PAH cations. *Nature*, 391:259.
- Thrower, J. D., Jørgensen, B., Friis, E. E., Baouche, S., Mennella, V., Luntz, A. C., Andersen, M., Hammer, B., and Hornekær, L. (2012). Experimental Evidence for the Formation of Highly Superhydrogenated Polycyclic Aromatic Hydrocarbons through H Atom Addition and Their Catalytic Role in H<sub>2</sub> Formation. *The Astrophysical Journal*, 752:3.
- Tielens, A. G. G. M. (2005). *The Physics and Chemistry of the Interstellar Medium*.
- Toennies, J. P., Welz, W., and Wolf, G. (1979). Molecular beam scattering studies of orbiting resonances and the determination of van der waals potentials for h–ne, ar, kr, and xe and for h<sub>2</sub>–ar, kr, and xe. *The Journal of Chemical Physics*, 71(2):614–642.
- Weingartner, J. C. and Draine, B. T. (2001). Photoelectric Emission from Interstellar Dust: Grain Charging and Gas Heating. *The Astrophysical Journal, Supplement*, 134:263–281.
- Wolfire, M. G., McKee, C. F., Hollenbach, D., and Tielens, A. G. G. M. (2003). Neutral Atomic Phases of the Interstellar Medium in the Galaxy. *The Astrophysical Journal*, 587:278–311.

# APPENDIX A

---

## Mass spectra

The mass spectra shown here are obtained after irradiating coronene cations with room temperature hydrogen atoms, except figure A.1. That figure shows the mass spectrum of coronene without any hydrogen addition. Figures A.2 through A.10 have been used in a quantitative analysis, while figures A.11 and A.12 are used in a qualitative manner.

For more details on the analysis, please have a look at chapter 6

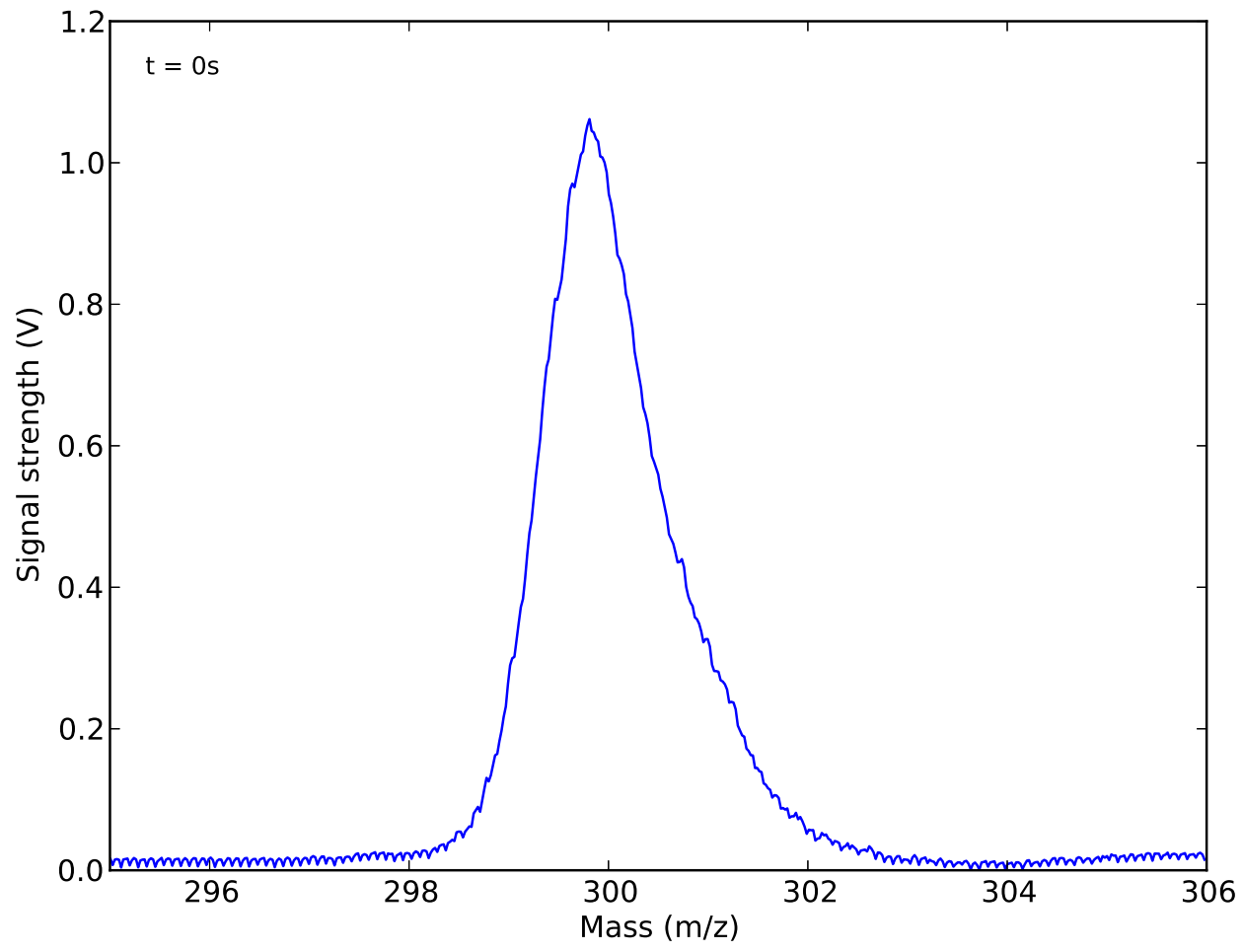


Figure A.1: The coronene mass spectrum without hydrogen irradiation.



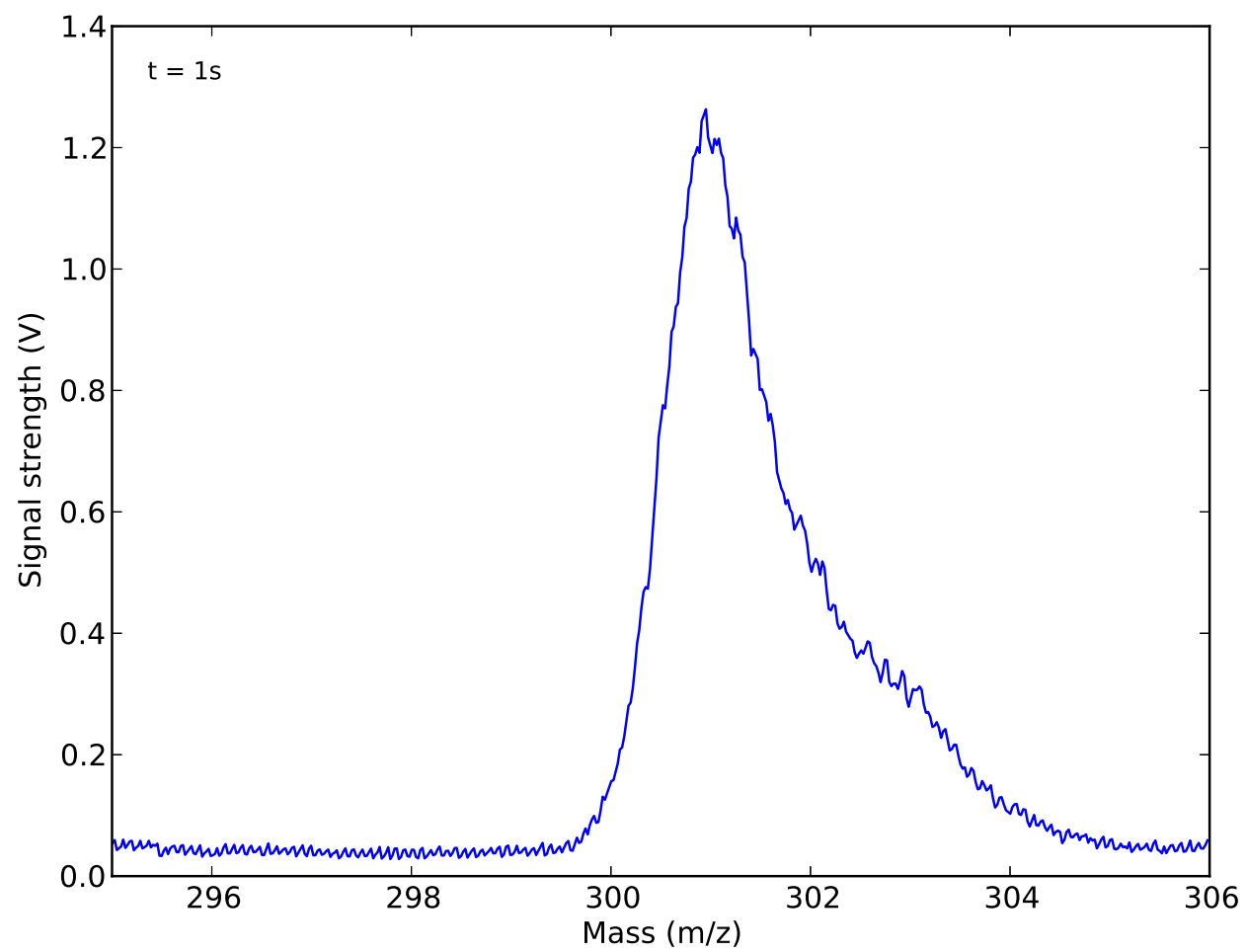


Figure A.2: The mass spectrum after irradiating coronene cations for 1 second.



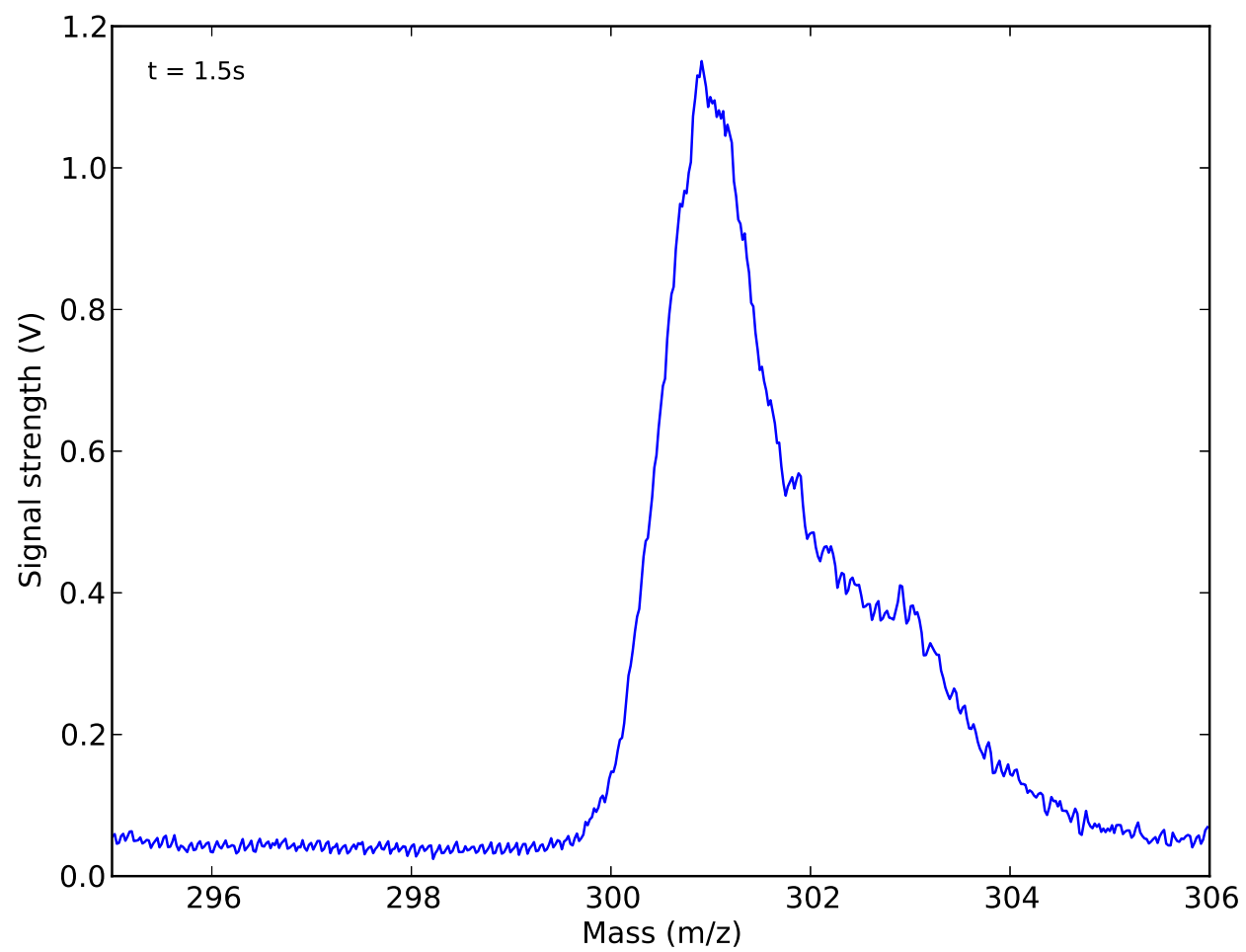


Figure A.3: The mass spectrum after irradiating coronene cations for 1.5 seconds.



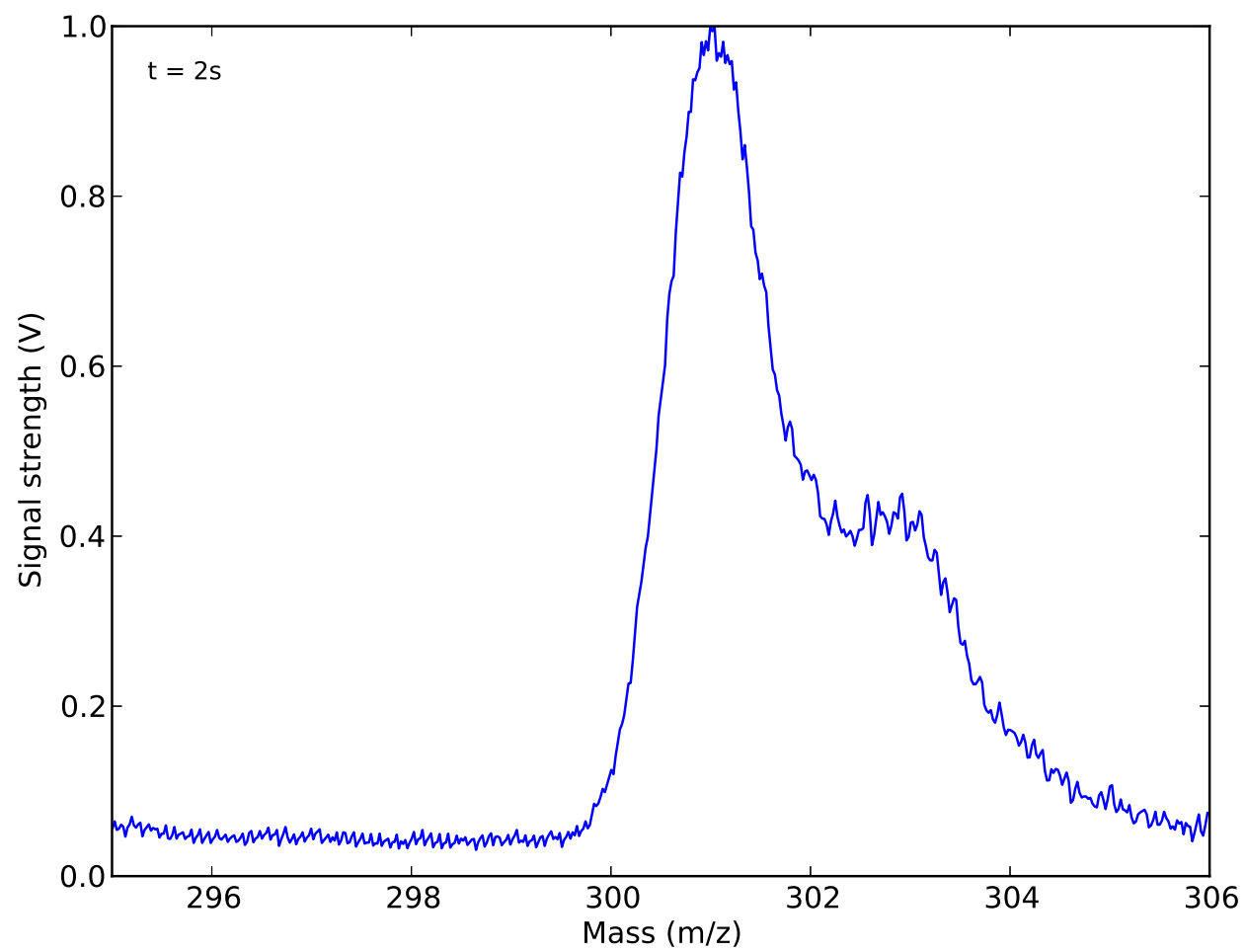


Figure A.4: The mass spectrum after irradiating coronene cations for 2 seconds.



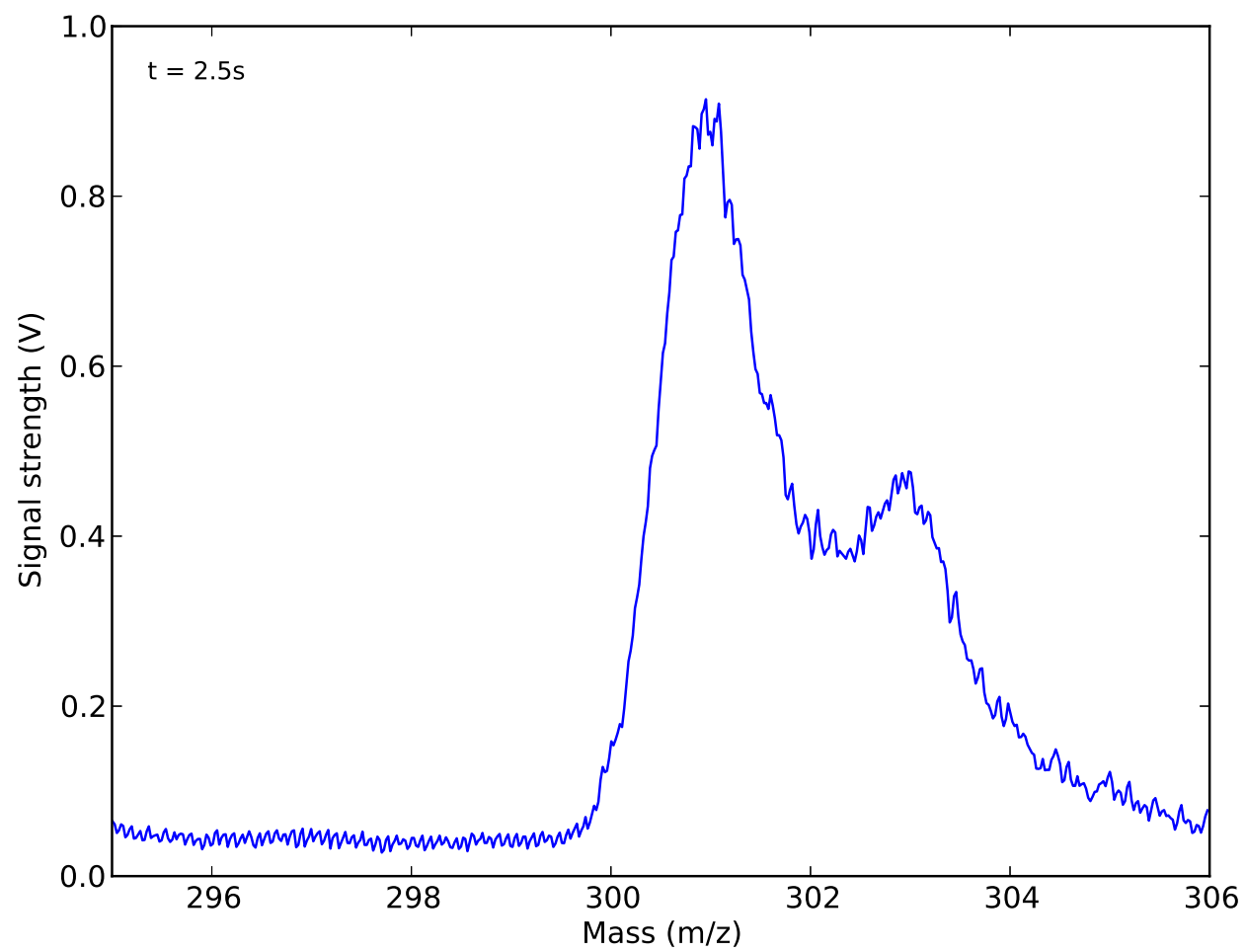


Figure A.5: The mass spectrum after irradiating coronene cations for 2.5 seconds.



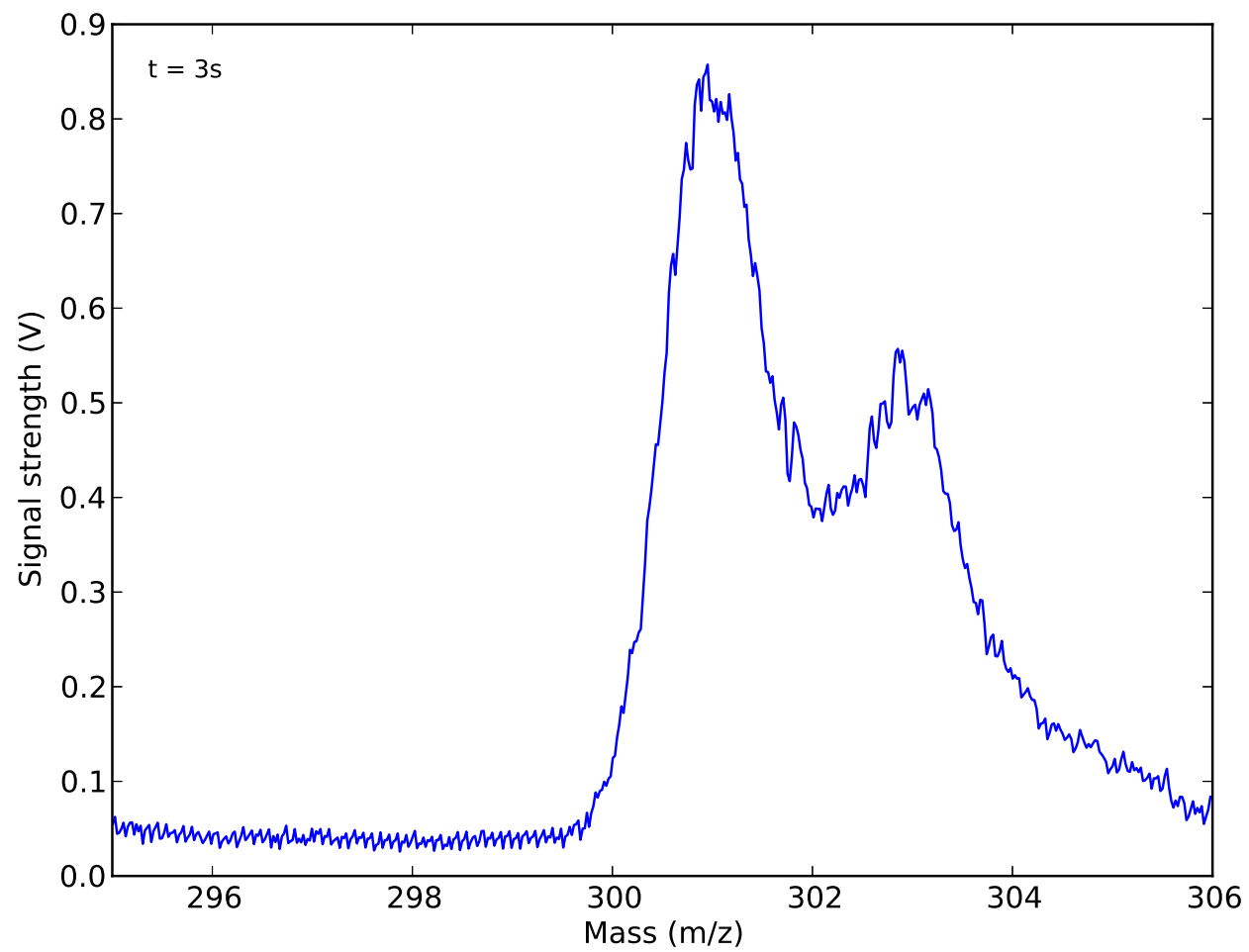


Figure A.6: The mass spectrum after irradiating coronene cations for 3 seconds.



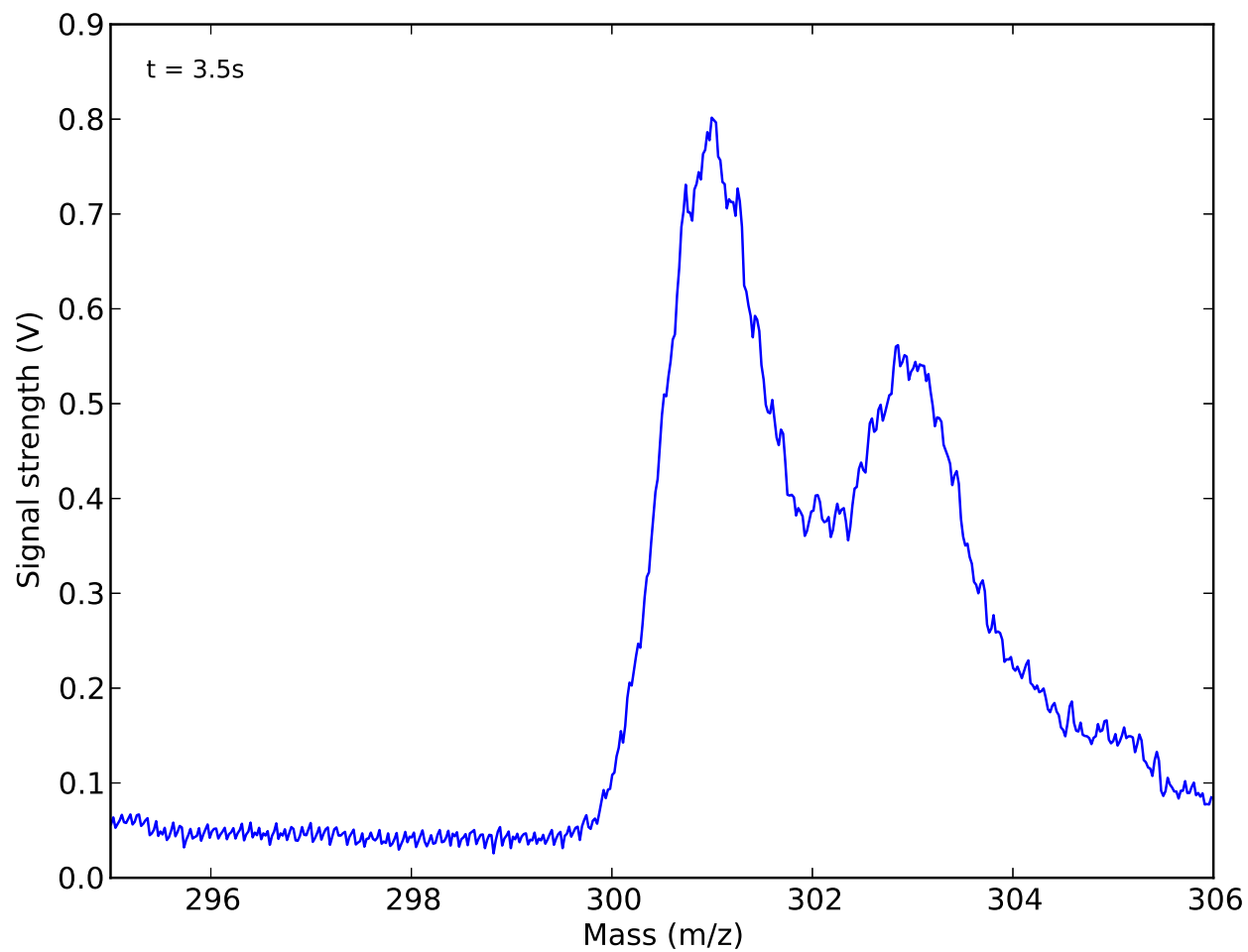


Figure A.7: The mass spectrum after irradiating coronene cations for 3.5 seconds.



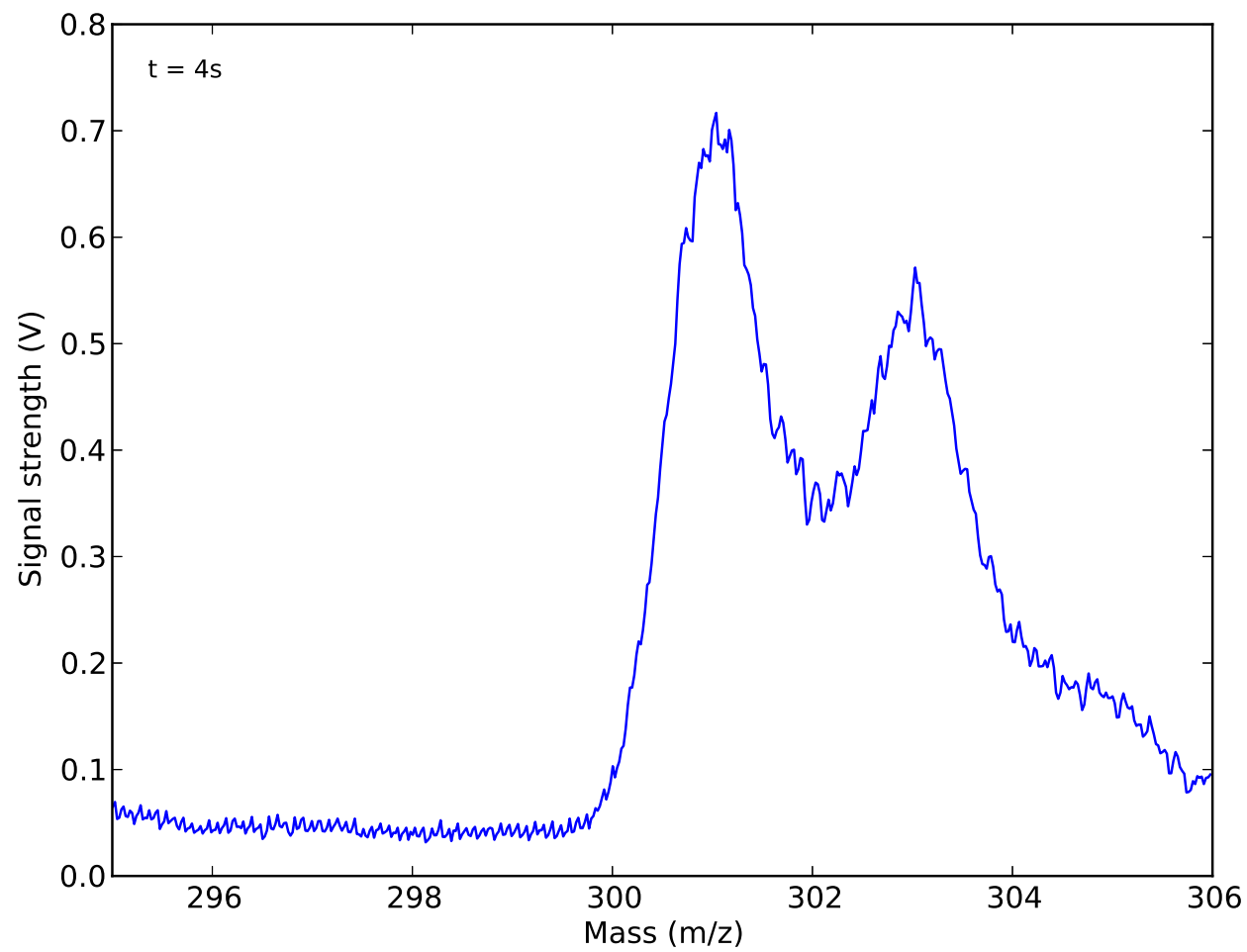


Figure A.8: The mass spectrum after irradiating coronene cations for 4 seconds.



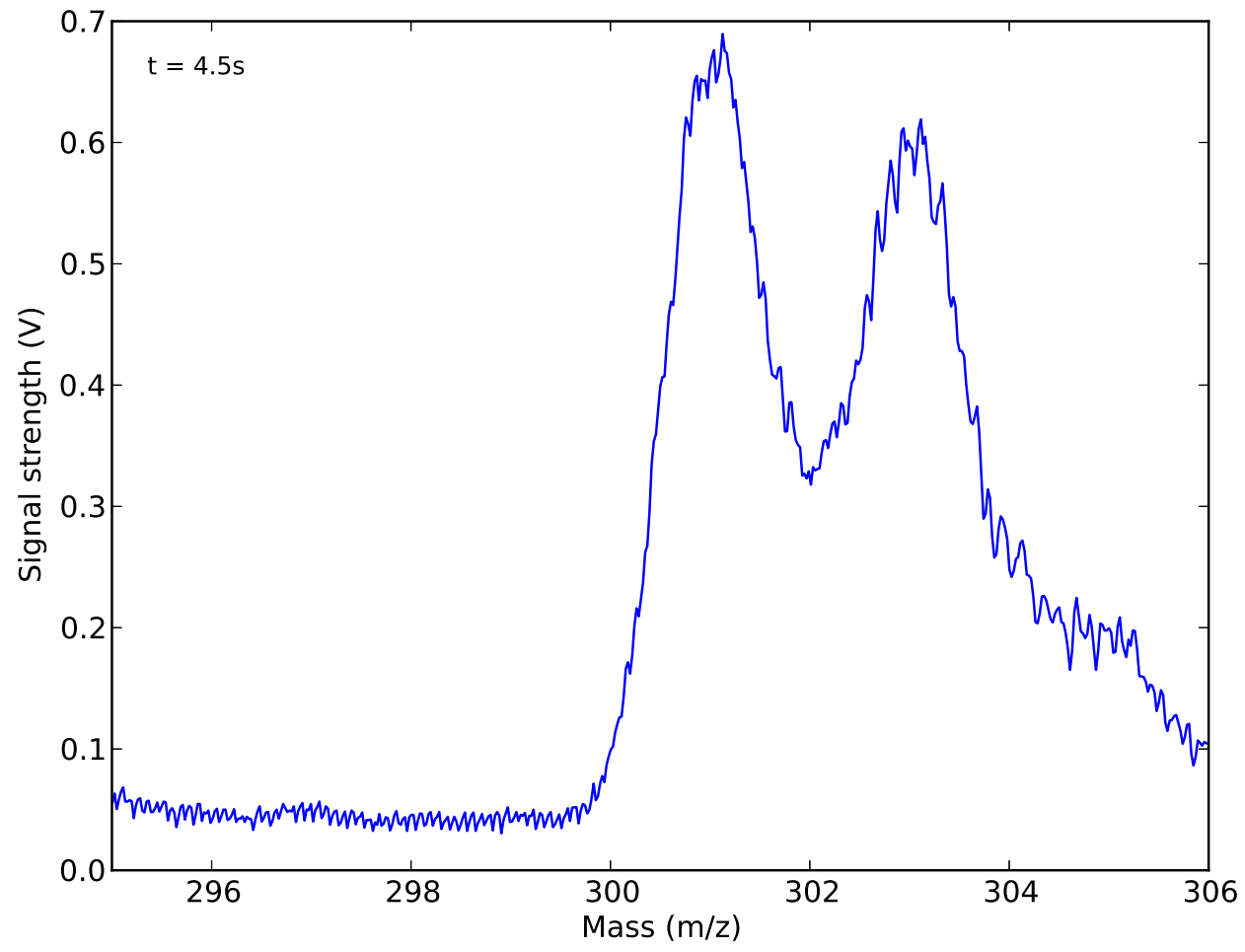


Figure A.9: The mass spectrum after irradiating coronene cations for 4.5 seconds.



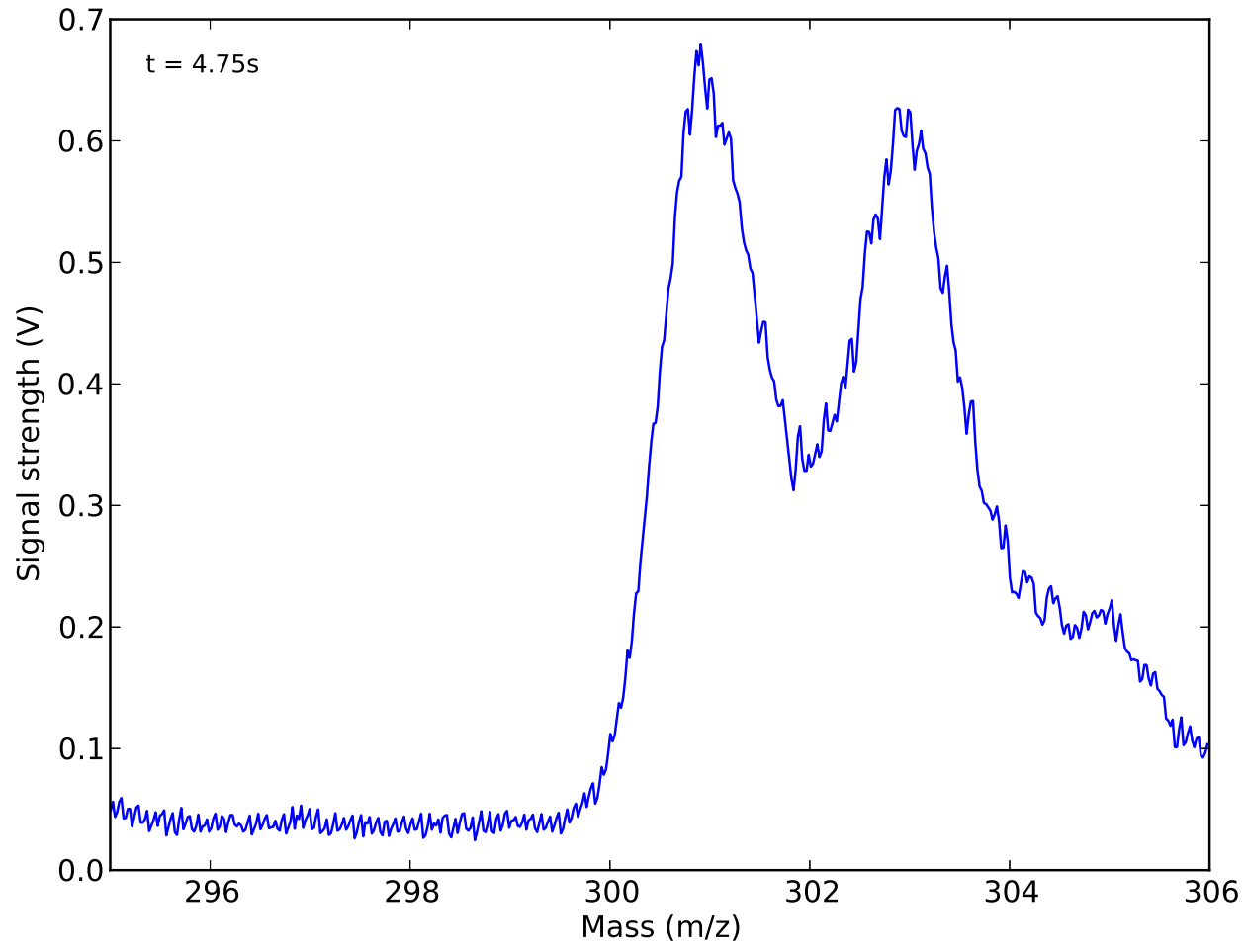


Figure A.10: The mass spectrum after irradiating coronene cations for 4.75 seconds.



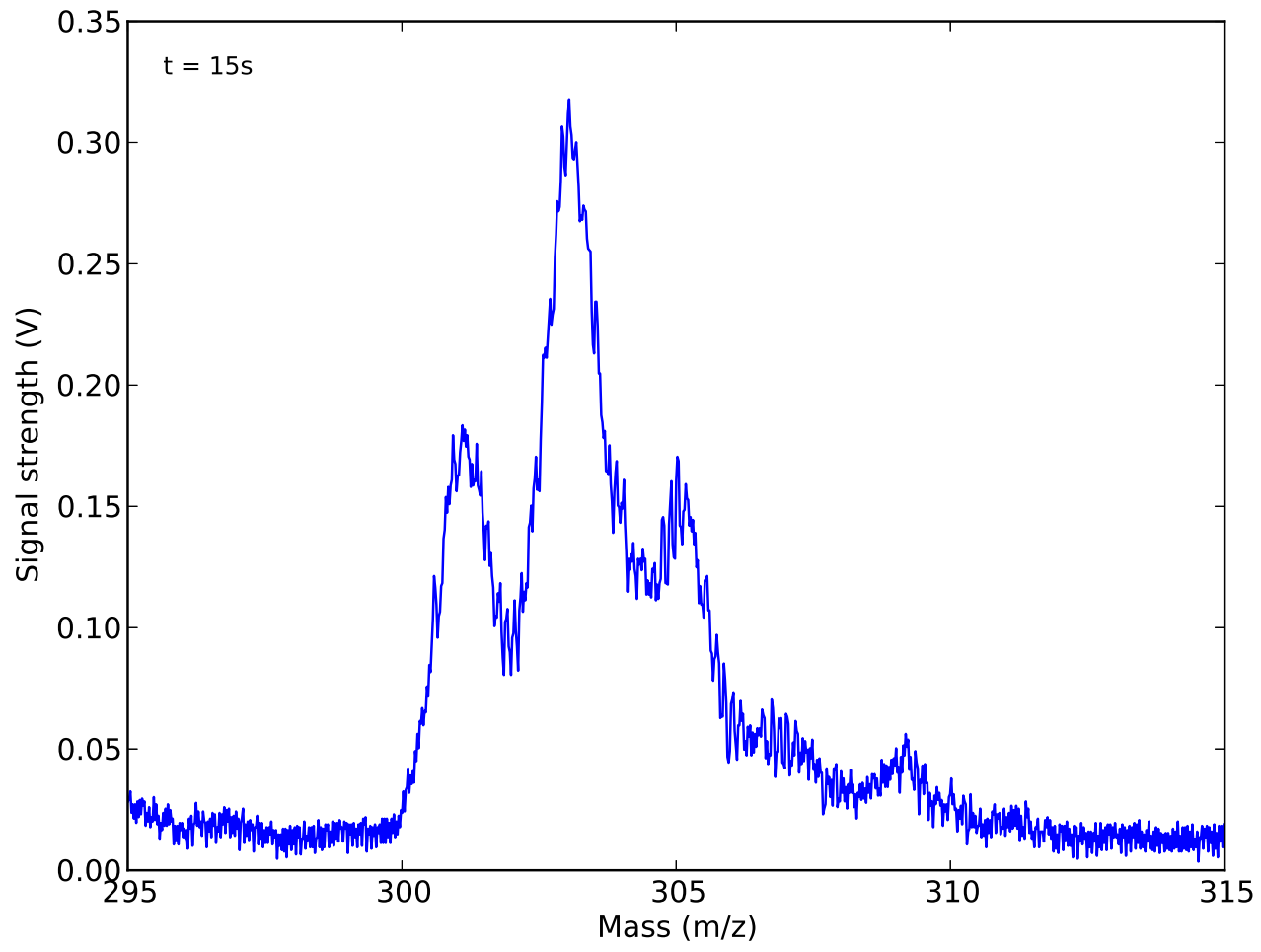


Figure A.11: The mass spectrum after irradiating coronene cations for 15 seconds.



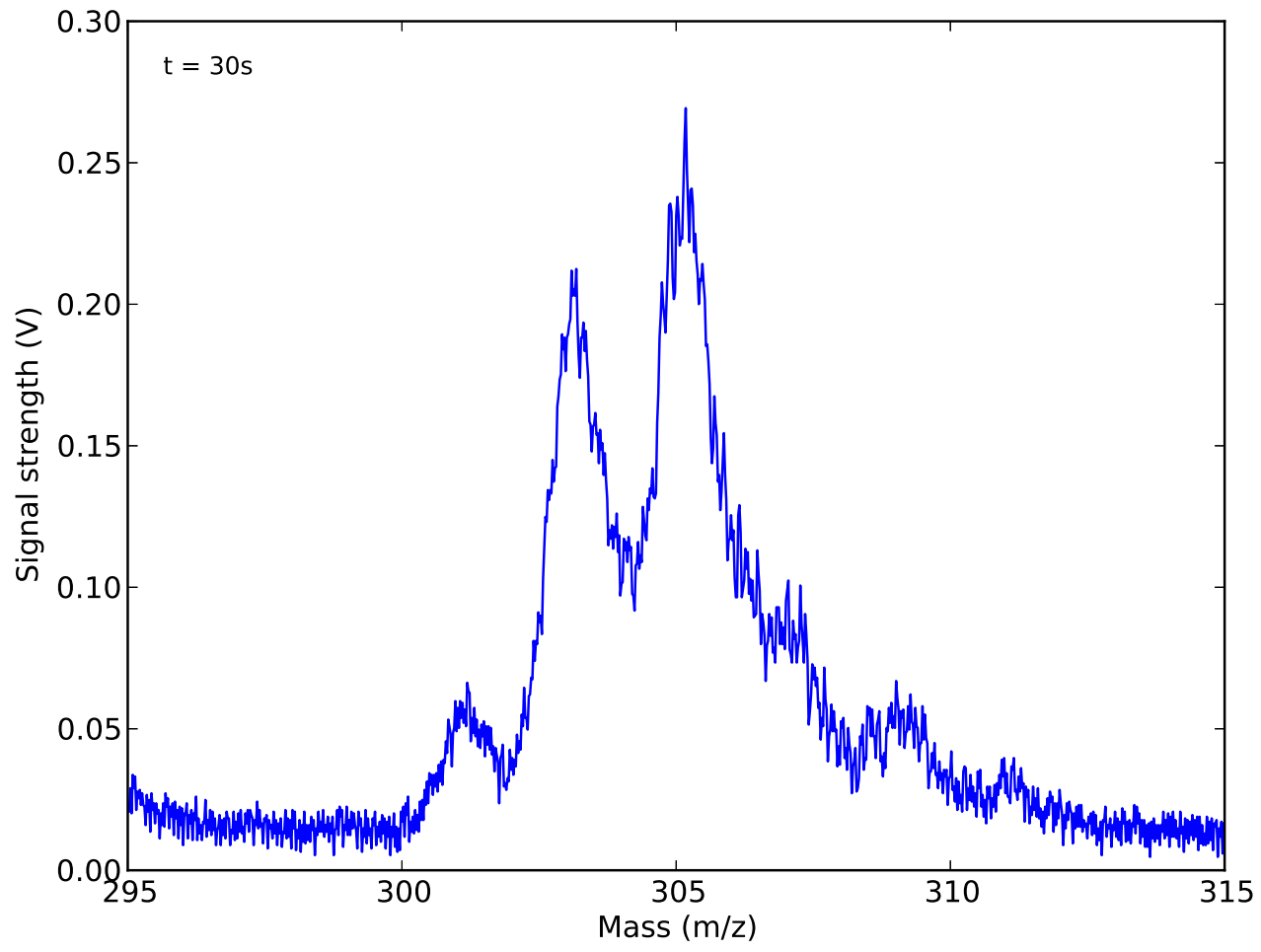


Figure A.12: The mass spectrum after irradiating coronene cations for 30 seconds.

## APPENDIX B Paper

The results that we present in this thesis have also been submitted as a Letter to the *Astrophysical Journal*, which was provisionally accepted. The manuscript with the minor changes was resubmitted on Monday November 19.

# Hydrogenation of PAH cations: a first step towards H<sub>2</sub> formation.

L. Boschman<sup>1,2</sup>, G. Reitsma<sup>2</sup>, S. Cazaux<sup>1</sup>, T. Schlathölter<sup>2</sup>, R. Hoekstra<sup>2</sup>, M. Spaans<sup>1</sup>  
and

O. González-Magaña<sup>2</sup>

boschman@astro.rug.nl

## ABSTRACT

Molecular hydrogen is the most abundant molecule in the universe. A large fraction of H<sub>2</sub> forms by association of hydrogen atoms adsorbed on polycyclic aromatic hydrocarbons (PAHs), where formation rates depend crucially on the H sticking probability. We have experimentally studied PAH hydrogenation by exposing coronene cations, confined in a radiofrequency ion trap, to gas phase atomic hydrogen. A systematic increase of the number of H atoms adsorbed on the coronene with the time of exposure is observed. Odd coronene hydrogenation states dominate the mass spectrum up to 11 H atoms attached. This indicates the presence of a barrier preventing H attachment to these molecular systems. For the second and fourth hydrogenation, barrier heights of  $72 \pm 6$  meV and  $40 \pm 10$  meV, respectively are found which is in good agreement with theoretical predictions for the hydrogenation of neutral PAHs. Our experiments however prove that the barrier does not vanish for higher hydrogenation states. These results imply that PAH cations, as their neutral counterparts, exist in highly hydrogenated forms in the interstellar medium. Due to this catalytic activity, PAH cations and neutrals seem to contribute similarly to the formation of H<sub>2</sub>.

*Subject headings:* astrochemistry — ISM: molecules

## 1. Introduction

Molecular hydrogen is the most abundant molecule in the universe and the main constituent of regions where stars are forming. H<sub>2</sub> plays an important role in the chemistry of the interstellar medium, and its formation governs the transformation of atomic diffuse clouds into molecular clouds. Because of the inefficient gas phase routes to form H<sub>2</sub>, dust grains have been recognized to be the favored habitat to form H<sub>2</sub> molecules (Oort & van de Hulst 1946, Gould & Salpeter 1963). The sticking of H atoms onto surfaces has received considerable attention because this mechanism governs the formation of H<sub>2</sub>, but also other molecules that contain H atoms. The sticking of

H atoms onto dust grains can also be an important mechanism to cool interstellar gas (Spaans & Silk 2000). In the past decades, a plethora of laboratory experiments and theoretical models have been developed to understand how H<sub>2</sub> forms. As H atoms arrive on dust surfaces, they can be weakly (physisorbed) or strongly (chemisorbed) bound to the surface. The sticking of H in the physisorbed state (Pirronello et al. 1997, 1999, 2000; Perry & Price 2003) and in the chemisorbed state (Zecho et al. 2002; Hornekær et al. 2006; Mennella 2006) has been highlighted by several experiments on different types of surfaces (amorphous carbon, silicates, graphite).

In the ISM, dust grains are mainly carbonaceous or silicate particles with various sizes and represent an important surface for the formation of H<sub>2</sub>. However, a large part ( $\sim 50\%$ ) of the available surface area for chemistry is in the form of very small grains or PAHs (Weingartner &

---

<sup>1</sup>Kapteyn Astronomical Institute, University of Groningen, P.O. Box 800, 9700 AV Groningen, the Netherlands

<sup>2</sup>KVI Atomic and Molecular Physics, University of Groningen, Zernikelaan 25, 9747 AA Groningen, the Netherlands.

Draine 2001). These PAHs are predicted to have characteristics similar to graphite surfaces: However, once the first H atom is chemisorbed on the basal plane, subsequent adsorptions of H atoms in pairs appear to be barrierless for the para dimer and with a reduced barrier for the ortho dimer (Rougeau et al. 2006). H<sub>2</sub> can then form by involving a pre-adsorbed H atom in monomer (Sha & Jackson 2002; Morisset et al. 2003; 2004b; Martinazzo & Tantardini 2006) or in a para-dimer configuration (Bachelier et al. 2007). However, while these routes represent efficient paths to form H<sub>2</sub>, the inefficient sticking of H atoms in monomers constitutes an important obstacle to enter the catalytic regime for H<sub>2</sub> formation. This results in a very low H<sub>2</sub> formation efficiency on graphitic/PAH surfaces (Cazaux et al. 2011).

The hydrogenation on the PAH edges has been identified as an important route to form H<sub>2</sub> in the ISM (Bauschlicher 1998; Hirama et al. 2004; Le Page et al. 2009; Mennella et al. 2012; Thrower et al. 2012). Density functional theory calculations have shown that the first hydrogenation of neutral coronene is associated with a barrier ( $\sim 60$  meV) but that subsequent hydrogenation barriers vanish (Rauls & Hornekær 2008). Recently, coronene films exposed to H/D atoms at high temperature, were studied by means of IR spectroscopy (Mennella et al. 2012) and mass spectrometry (Thrower et al. 2012). These measurements showed that neutral PAHs, when highly hydrogenated, are efficient catalysts for the formation of H<sub>2</sub>, and confirmed the high H<sub>2</sub> formation rate attributed to PAHs in PDRs (Mennella et al. 2012).

PAH cations, which are usually present at lower extinction  $A_V$ , and therefore reside at the surfaces of PDRs, also represent an important route to form H<sub>2</sub> (Bauschlicher 1998; Le Page et al. 2009). The addition of the first H atom is predicted to be barrierless. This reaction is exothermic but the product should be stabilized by IR emission. A second H atom can react with the already adsorbed H to form H<sub>2</sub> without a barrier (Bauschlicher 1998; Hirama et al. 2004).

In this letter, we study experimentally the hydrogenation of coronene cations in the gas phase through exposure to hydrogen atoms. By using mass spectrometry, we show that odd hydrogenation states of coronene cations predominantly pop-

ulate the mass spectrum. Our results highlight the fact that the further hydrogenation of PAH cations is associated with a barrier if the number already attached H atoms is odd, and no barrier if this number is even. This alternanting barrier-no barrier occurrence seems to remain with increasing hydrogenation. These results suggest that PAH cations can also enjoy highly hydrogenated states in the interstellar medium, and acts as catalysts for H<sub>2</sub> formation.

## 2. Experiments

In this pilot experiment we show the feasibility of studying the hydrogenation of PAHs in the gas phase. For this purpose, we use a setup designed to study molecular ions in a radiofrequency ion trap. Time-of-flight mass spectrometry of the trap content is used to identify the changes in mass of the coronene cations and therefore deduce their respective degrees of hydrogenation.

### 2.1. Set-up

The experiments have been performed using a home-built tandem-mass spectrometer shown schematically in figure 1 (Bari et al. 2011). A beam of singly charged coronene radical cations ( $[\text{C}_{24}\text{H}_{12}]^+$ ,  $m/z$  300) was extracted from an electrospray ion source. The ions were phase-space compressed in an radiofrequency (RF) ion funnel and subsequently in an RF quadrupole ion guide. Mass selection was accomplished by using an RF quadrupole mass filter. Accumulation of the ions took place in a three dimensional RF ion trap (Paul trap). A He buffer gas at room temperature was used to collisionally cool the trapped cations. Exposure to gas-phase atomic hydrogen for variable periods of time led to multiple hydrogen adsorption on the coronene cations. An electric extraction field was then applied between the trap end-caps to extract the trapped hydrogenated cations into a time-of-flight (TOF) mass spectrometer with resolution  $M/\Delta M \sim 200$ . To obtain mass spectra of sufficient statistics, typically a couple of hundred TOF traces were accumulated.

Electrospray ionization allows to gently transfer ions from the liquid phase into the gas phase. Inspired by the method of Maziarz (2005) we have run the ion source with a solution consisting of 600  $\mu\text{L}$  of saturated solution of coronene in methanol,

350  $\mu\text{L}$  of HPLC grade methanol and 50  $\mu\text{L}$  of 10 mM solution of  $\text{AgNO}_3$  solution in methanol. In the liquid phase, electron transfer from a coronene molecule to a silver ion leads to formation of the required radical cation.

The trapped ions are exposed to hydrogen atoms produced from  $\text{H}_2$  by a Slevin type source which has been extensively used in crossed beam experiments (Hoekstra et al. 1991, Blik et al. 1997). While in the earlier work the dissociation fractions were determined by means of electron impact excitation or HeII line emission, we now use charge removal (captured ionization) and dissociation induced by 40 keV  $\text{He}^{2+}$ . For these processes the cross sections are well-known (Shah & Gilbody 1978). In this way we determine a hydrogen dissociation fraction of  $n(\text{H}) / (n(\text{H}) + n(\text{H}_2)) \approx 0.3$ . The temperature of the H beam is around room temperature ( $\sim 25$  meV).

## 2.2. Results

Coronene ions are exposed to a constant flux of H atoms for different periods of time before their degree of hydrogenation is determined by means of mass spectrometry. The irradiation time is varied from 1.0 up to 30 s to study the time-dependence of coronene hydrogenation.

The data obtained from our experiment are a series of mass spectra of hydrogenated coronene cations as a function of H exposure time. Some of the spectra are shown in fig.2. Fig.2(a) shows the mass spectrum of the native  $m/z=300$  coronene cations. A similar, thus unchanged, mass spectrum is obtained (not shown in this article) if we

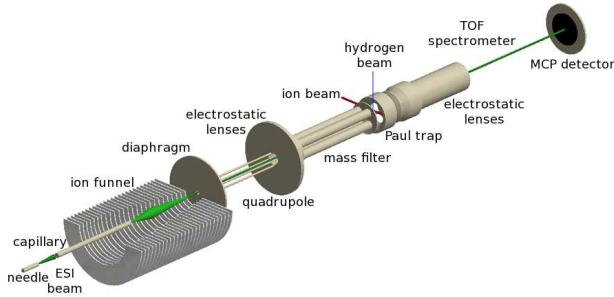


Fig. 1.— The setup used, with the ion funnel, quadrupoles, ion trap, hydrogen source and detector

irradiate coronene cations with molecular hydrogen. This means that molecular hydrogen does not stick to coronene cations at room temperature.

After turning on the hydrogen source and exposing the coronene cations to the atomic hydrogen beam for 1.0 s (fig.2, (b)), the peak at  $m/z = 300$  shifts to 301, which means that the trap content main constituent is  $(\text{C}_{24}\text{H}_{12}+\text{H})^+$ . For increasing irradiation time (fig.2(c)  $t= 2$  s, (d) 3 s, (e) 4 s and (f) 4.75 s), the peak at  $m/z=301$  disappears progressively while a peak at  $m/z = 303$  and then at  $m/z = 305$  (for  $t = 4.75$  s see fig.2(f)) appears, which indicates the addition of 3 and 5 hydrogen atoms, respectively. At longer exposure time (fig.3(a)  $t \sim 15$  s), the  $m/z=303$  peak dominates the signal, and a peak at  $m/z=305$  appears. At even longer irradiation times (fig.3(b)  $t \sim 30$  s), the peak  $m/z=305$  dominates and peaks at  $m/z=307$  and 309 appear. These peaks clearly show the evolution of the hydrogenation states of coronene cations with H irradiation time.

## 3. Analysis and discussion

Our results show that the most important peaks measured in the mass spectrum shift from lower masses to higher masses with increasing H exposure time. In order to follow the evolution of the first hydrogenated state of coronene cation  $(\text{C}_{24}\text{H}_{12}+\text{H})^+$  ( $\text{CorH}^+$ ) to the second  $(\text{C}_{24}\text{H}_{12}+2\text{H})^+$  ( $\text{CorH}_2^+$ ), third ( $\text{CorH}_3^+$ ) and fourth ( $\text{CorH}_4^+$ ) hydrogenated states, we use a simple model that describes this evolution :

$$\frac{d n_{\text{CorH}^+}}{dt} = - \left( A_2 e^{-\frac{E_2}{k_B T_{\text{gas}}}} n_{\text{CorH}^+} \right) n_H \quad (1)$$

$$\frac{d n_{\text{CorH}_2^+}}{dt} = \left( A_2 e^{-\frac{E_2}{k_B T_{\text{gas}}}} n_{\text{CorH}^+} - A_3 n_{\text{CorH}_2^+} \right) n_H \quad (2)$$

$$\frac{d n_{\text{CorH}_3^+}}{dt} = \left( A_3 n_{\text{CorH}_2^+} - A_4 e^{-\frac{E_4}{k_B T_{\text{gas}}}} n_{\text{CorH}_3^+} \right) n_H \quad (3)$$

$$\frac{d n_{\text{CorH}_4^+}}{dt} = \left( A_4 e^{-\frac{E_4}{k_B T_{\text{gas}}}} n_{\text{CorH}_3^+} - A_5 n_{\text{CorH}_4^+} \right) n_H \quad (4)$$

Hydrogenation of  $\text{CorH}_{2n+1}^+$  follows an Arrhenius expression where  $A_{2n+2}$  is the prefactor and  $E_{2n+2}$  is the barrier, while hydrogenation of

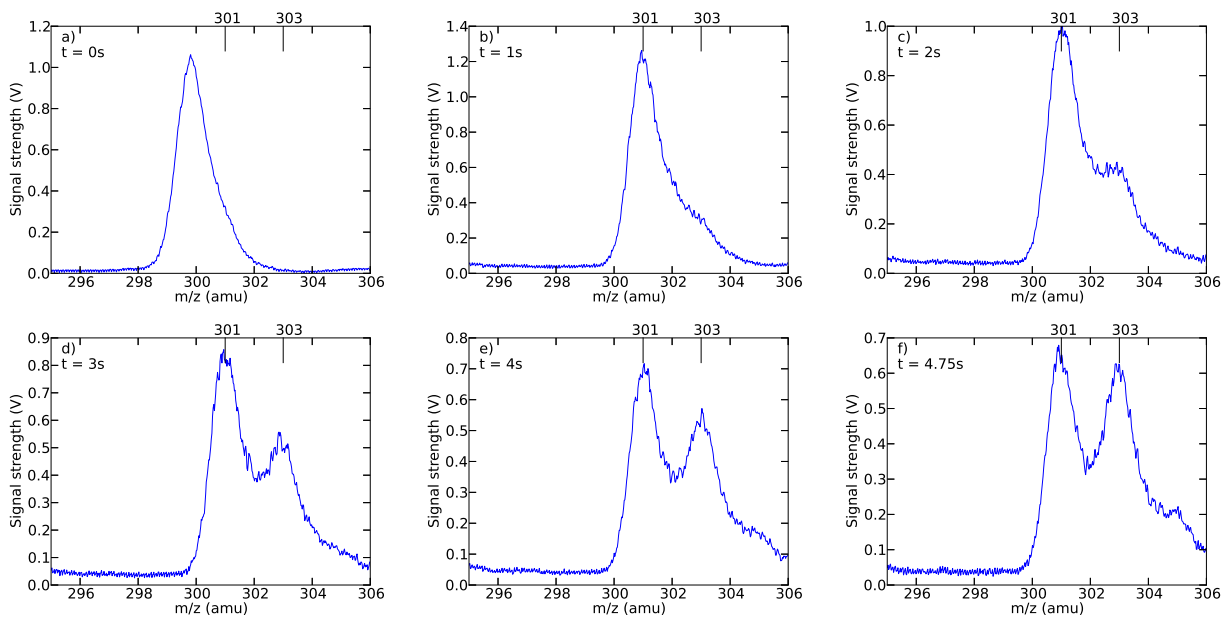


Fig. 2.— Mass spectrum of coronene a) without and with exposure to H atoms during b) 1 s c) 2 s d) 3 s e) 4 s f) 4.5 s.

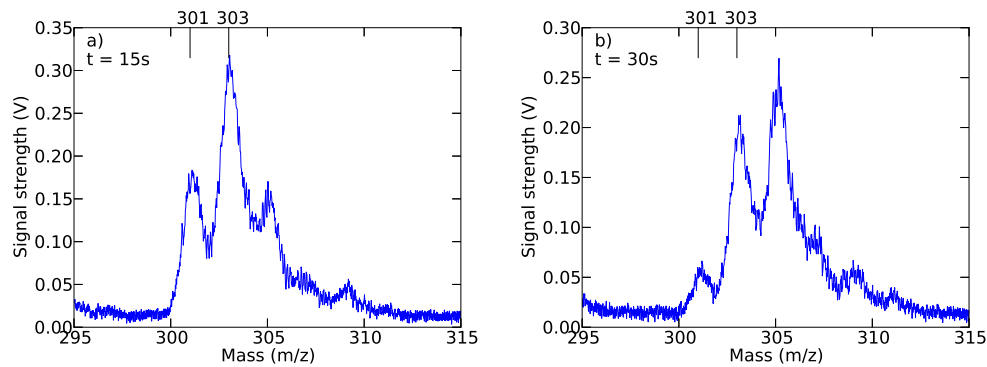


Fig. 3.— Same as fig.2 for much longer H exposures of a) 15 s b) 30 s.

$\text{CorH}_{2n}^+$  follows the same expression with a prefactor  $A_{2n+1}$  and no barrier.  $k_B$  is the Boltzmann constant and  $T$  the temperature of the H beam ( $T \sim 25$  meV).

In these equations we do not include abstraction, meaning that the time evolution of the contribution of each state is governed entirely by hydrogenation. This assumption is made in order to derive the first barriers of hydrogenation. Abstraction can be neglected in the conditions of our experiments for low exposure times. This is supported by previous experiments where the cross section for addition of hydrogen to neutral coronene is predicted to be 20 times that for abstraction (Mennella et al. 2012). Further support is drawn from a kinetic chemical model we developed, which shows that abstraction has to be very low compared to hydrogenation to be able to mimic the experimental results (Boschman et al. in prep). However, for long H exposure time we expect the hydrogenation degree of the coronene cations to reach a steady state which will allow us to derive the contribution of abstraction relative to addition, and therefore derive the  $\text{H}_2$  formation rate due to PAH cations. It should also be kept in mind that in the conditions of our experiments, the H atoms are at room temperature meaning that they cross the barriers for abstraction (10 meV, Rauls & Hornekær 2008) and addition (40 - 60 meV, Rauls & Hornekær 2008) with similar ease. Under interstellar conditions, however, the abstraction will dominate by 8 orders of magnitude (at 20 K) because of the barrier differences.

The first hydrogenation is expected to take place at the outer edge carbon atom (Hirama et al. 2004). This state provides more conformational freedom to the four neighbouring outer edge carbon atoms, ensuring a preference for the second hydrogenation to take place at one of those four carbon atoms. The third hydrogenation will preferentially take place at the outer edge carbon next to the second H atom. Again, the fourth H atom can be bound to one of the four neighbouring outer edge carbon atoms, and the fifth sticks on the neighboring outer edge carbon. This scenario of H atoms sticking preferentially on outer edge carbons next to already adsorbed atoms is described in Rauls & Hornekær (2008).

The contribution of every peak is determined by fitting our data with Gaussians with identical

widths (see fig.4(a)). The ratios between different hydrogenation states as function of time are reported in fig.4(b). It appears that the ratio between the contribution of the first ( $\text{CorH}^+$ ) and the second ( $\text{CorH}_2^+$ ) hydrogenation state does not evolve with time for short time scales ( $\frac{n_{\text{CorH}^+}}{n_{\text{CorH}_2^+}} \sim 3$  until 5s). Also, the ratio between the third ( $\text{CorH}_3^+$ ) and the fourth ( $\text{CorH}_4^+$ ) hydrogenation state shows identical behaviour after  $t \geq 2$ s ( $\frac{n_{\text{CorH}_3^+}}{n_{\text{CorH}_4^+}} \sim 3$  from 2s onwards). Before this exposure time the  $n_{\text{CorH}_3^+}$  and  $n_{\text{CorH}_4^+}$  signals are very weak, and the ratio is uncertain. We can therefore assume that for these measurements  $\frac{d}{dt} \left( \frac{n_{\text{CorH}_2^+}}{n_{\text{CorH}^+}} \right) = 0$  and  $\frac{d}{dt} \left( \frac{n_{\text{CorH}_3^+}}{n_{\text{CorH}_4^+}} \right) = 0$ . The expression for the  $\text{CorH}^+$  to  $\text{CorH}_2^+$  as well as for the  $\text{CorH}_3^+$  to  $\text{CorH}_4^+$  energy barriers can then be written as:

$$E_2 = -k_B T_{\text{gas}} \ln \left( \frac{A_3}{A_2} \frac{1}{1 + \frac{n_{\text{CorH}^+}}{n_{\text{CorH}_2^+}}} \right) \quad (5)$$

$$E_4 = -k_B T_{\text{gas}} \ln \left( \frac{A_5 + A_3 \frac{n_{\text{CorH}_2^+}}{n_{\text{CorH}_3^+}}}{A_4} \frac{1}{1 + \frac{n_{\text{CorH}_3^+}}{n_{\text{CorH}_4^+}}} \right) \quad (6)$$

From these expressions we derive the energy barrier  $E_2$  as  $72 \pm 6$  meV and  $E_4$  as  $43 \pm 8$  meV, as shown in fig.4(c). This shows that hydrogenation barriers are decreasing with increasing hydrogenation. However, our results also show that odd hydrogenated states dominate the mass spectrum even for high degrees of hydrogenation (fig.3). This highlights the presence of a barrier-no barrier alternation from one hydrogenated state to another, up to high hydrogenation states. So our results indicate that even if the hydrogenation barriers decrease for the first hydrogenations, they do not vanish completely and remain at higher hydrogenation states. The barriers derived in our study are similar to the one calculated by Rauls & Hornekær (2008) for neutral coronene. This means that the first hydrogenations of coronene cations should be comparable to the hydrogenation of neutral coronene. However, for higher degree of hydrogenation we show that these barriers still exist, while the calculations from Rauls &

Hornekær (2008) predict that these barriers vanish after a few hydrogenations. Recent mass spectrometric measurements of coronene films exposed to H/D atoms do not show preferences for even or odd hydrogenation states of neutral coronene (Thrower et al. 2012). However, these measurements are not very sensitive to barrier heights well below 100 meV, since the experiments were performed with atoms at beam temperature of 170 meV.

In PDRs exposed to UV fields less than few hundreds  $G_0$ , the spatial distribution of  $H_2$  and PAHs does correlate (Habart et al. 2003, Habart et al. 2005, Compiègne et al. 2007) contrary to what is seen in the presence of strong UV fields (Tielens et al. 1993, Berné et al. 2009). The  $H_2$  formation rates have been derived for several PDRs exposed to various UV radiation fields. These rates can be explained by the contribution of PAHs to the formation of  $H_2$  (Habart et al. 2004). Depending on the UV intensity, the PAHs observed can either be PAH cations, that are present in regions at low visual extinctions  $A_V$ , or neutral PAHs, which are located at higher extinctions. Work by Wolfire et al. (2008) and Spaans & Meijerink (2005) has shown that high-UV and high density PDRs ( $n_H \geq 10^3 \text{ cm}^{-3}$  and  $G_0 \geq 100$ ,  $G_0 = 1.6 \times 10^{-3} \text{ erg cm}^{-3} \text{ s}^{-1}$ ) can maintain a  $\sim 30\%$  cationic fraction upto a few mag in  $A_V$ . More relevant to this work, Cox & Spaans (2006) have studied low-UV PDRs ( $G_0 \leq 100$ ), and followed the PAH charge balance for different densities, UV radiation fields and metallicities. They found that PAH cations dominate over neutrals and anions for  $A_V \leq 2$  mag. The  $H_2$  formation rates observed in PDRs exposed to different UV fields can therefore be partly attributed to neutral and cationic PAHs.

Our results show that the hydrogenation processes of neutral and cationic PAHs are similar and should contribute similarly to the formation of  $H_2$ . Further experimental investigations will allow us to derive the  $H_2$  formation rate for PAH cations.

#### 4. Conclusions

We have investigated the addition of hydrogen atoms to coronene cations in the gas phase and observed increasing hydrogenation with H exposure

time. Our results show that odd hydrogenated states dominate the mass spectrum, which evidences the presence of a barrier for the further hydrogenation of odd hydrogenation states. The first hydrogen sticks to the coronene cations without a barrier (Snow et al. 1998, Hirama et al. 2004). The second and forth hydrogenations are associated with barriers of about  $72 \pm 6$  meV and  $43 \pm 8$  meV, while the third and fifth hydrogenation are barrierless. These barriers are similar to the one calculated for neutral coronene (Rauls & Hornekær 2008). Our results indicate that super-hydrogenated PAH cations (Li & Draine (2012)) should also be found in the interstellar medium, and be important catalysts for the formation of  $H_2$ , as it is the case for their neutral counterparts.

#### ACKNOWLEDGMENTS

L. B. and S. C. are supported by the Netherlands Organization for Scientific Research (NWO). G.R. recognizes the funding by the NWO Dutch Astrochemistry Network. We would like to thank the anonymous referee for the helpful comments.

#### REFERENCES

- Bachelier, D., Sizun, M., Teillet-Billy, D., Rougeau, N., & Sidis, V. 2007, *Chemical Physics Letters*, 448, 223
- Bari, S., Gonzalez-Magana, O., Reitsma, G., et al. 2011, *The Journal of Chemical Physics*, 134, 024314
- Bauschlicher, Jr., C. W. 1998, *ApJ*, 509, L125
- Berné, O., Fuente, A., Goicoechea, J. R., et al. 2009, *ApJ*, 706, L160
- Blik, F., Woestenenk, G., Hoekstra, R., & Morgenstern, R. 1997, *Hyperfine Interactions*, 108, 121
- Cazaux, S., Morisset, S., Spaans, M., & Allouche, A. 2011, *A&A*, 535, A27
- Compiègne, M., Abergel, A., Verstraete, L., et al. 2007, *A&A*, 471, 205
- Cox, N. L. J. & Spaans, M. 2006, *A&A*, 451, 973
- Gould, R. J. & Salpeter, E. E. 1963, *ApJ*, 138, 393

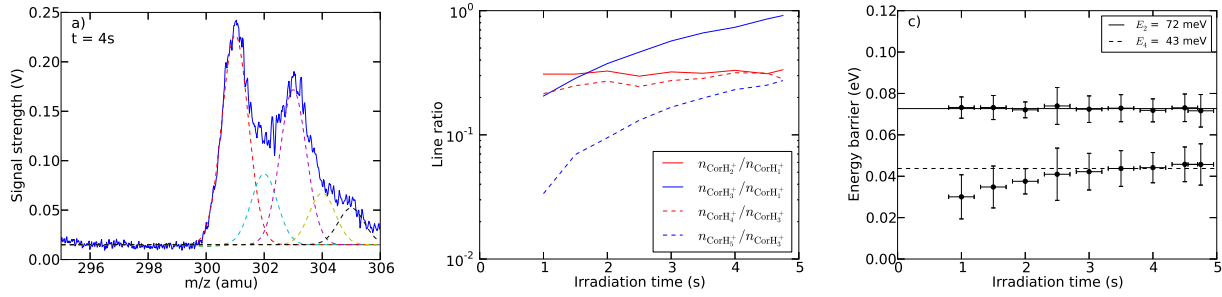


Fig. 4.— a) Contribution of every peak determined by fitting our data with Gaussians with identical widths. b) Ratios between different hydrogenation states as function of time. c) Barrier heights for the second and fourth hydrogenations.

- Habart, E., Abergel, A., Walmsley, C. M., Teyssier, D., & Pety, J. 2005, *A&A*, 437, 177
- Habart, E., Boulanger, F., Verstraete, L., et al. 2003, *A&A*, 397, 623
- Habart, E., Boulanger, F., Verstraete, L., Walmsley, C. M., & Pineau des Forêts, G. 2004, *A&A*, 414, 531
- Hirama, M., Tokosumi, T., Ishida, T., & ichi Aihara, J. 2004, *Chemical Physics*, 305, 307
- Hoekstra, R., de Heer, F. J., & Morgenstern, R. 1991, *Journal of Physics B: Atomic, Molecular and Optical Physics*, 24, 4025
- Hornekær, L., Rauls, E., Xu, W., et al. 2006, *Physical Review Letters*, 97, 186102
- Le Page, V., Snow, T. P., & Bierbaum, V. M. 2009, *ApJ*, 704, 274
- Li, A. & Draine, B. T. 2012, *ArXiv e-prints*, 1210.6558
- Martinazzo, R. & Tantardini, G. F. 2006, *Journal of Chemical Physics*, 124
- Maziarz, E. 2005, *Canadian Journal of Chemistry - Revue Canadienne de Chimie*, 85, 1871
- Mennella, V. 2006, *ApJ*, 647, L49
- Mennella, V., Hornekær, L., Thrower, J., & Accolla, M. 2012, *ApJ*, 745, L2
- Morisset, S., Aguillon, F., Sizun, M., & Sidis, V. 2003, *Chemical Physics Letters*, 378, 615
- Morisset, S., Aguillon, F., Sizun, M., & Sidis, V. 2004b, *The Journal of Physical Chemistry A*, 108, 8571
- Oort, J. H. & van de Hulst, H. C. 1946, *Bull. Astron. Inst. Netherlands*, 10, 187
- Perry, J. S. A. & Price, S. D. 2003, *Ap&SS*, 285, 769
- Pirronello, V., Biham, O., Manicó, G., Roser, J. E., & Vidali, G. 2000, in *Molecular Hydrogen in Space*, ed. F. Combes & G. Pineau Des Forets, 71–+
- Pirronello, V., Liu, C., Roser, J. E., & Vidali, G. 1999, *A&A*, 344, 681
- Pirronello, V., Liu, C., Shen, L., & Vidali, G. 1997, *ApJ*, 475, L69+
- Rauls, E. & Hornekær, L. 2008, *ApJ*, 679, 531
- Rougeau, N., Teillet-Billy, D., & Sidis, V. 2006, *Chemical Physics Letters*, 431, 135
- Sha, X. & Jackson, B. 2002, *Surface Science*, 496, 318
- Shah, M. B. & Gilbody, H. B. 1978, *Journal of Physics B Atomic Molecular Physics*, 11, 121
- Snow, T. P., Le Page, V., Keheyang, Y., & Bierbaum, V. M. 1998, *Nature*, 391, 259
- Spaans, M. & Meijerink, R. 2005, *Ap&SS*, 295, 239
- Spaans, M. & Silk, J. 2000, *ApJ*, 538, 115

Thrower, J. D., Jørgensen, B., Friis, E. E., et al.  
2012, ApJ, 752, 3

Tielens, A. G. G. M., Meixner, M. M., van der  
Werf, P. P., et al. 1993, Science, 262, 86

Weingartner, J. C. & Draine, B. T. 2001, ApJ,  
548, 296

Wolfire, M. G., Tielens, A. G. G. M., Hollenbach,  
D., & Kaufman, M. J. 2008, ApJ, 680, 384

Zecho, T., Guttler, A., Sha, X., Jackson, B., &  
Kuppers, J. 2002, J. Chem. Phys., 117, 8486